Materials Science & Engineering C 121 (2021) 111838

Contents lists available at ScienceDirect

Materials Science & Engineering C

journal homepage: www.elsevier.com/locate/msec

Adjustable conduits for guided peripheral nerve regeneration prepared from bi-zonal unidirectional and multidirectional laminar scaffold of type I collagen

Diana Millán [a,b,1], Ronald A. Jiménez [a,c,1], Luis E. Nieto [e], Ivan Y. Poveda [a], Maria A. Torres [a], Ana S. Silva [d], Luis F. Ospina [f], João F. Mano [d], Marta R. Fontanilla [a,*]

[a] Tissue Engineering Group, Department of Pharmacy, Universidad Nacional de Colombia, Av. Carrera 30 # 45-10, 111321 Bogotá, Colombia
[b] Universidad El Bosque, Facultad de Medicina, Colombia
[c] Universidad El Bosque, Facultad de Ciencias, Colombia
[d] Department of Chemistry, CICECO, University of Aveiro, Campus Universitário de Santiago, 3810-193 Aveiro, Portugal
[e] Facultad de Medicina, Pontificia Universidad Javeriana, Carrera 7 # 40-62 Of 726, Bogotá, Colombia
[f] Department of Pharmacy, Universidad Nacional de Colombia, 111321, Av. Carrera 30 # 45-10, Bogotá, Colombia

ARTICLE INFO

Keywords:
Bi-zonal scaffolds
Collagen type I
Peripheral nerve regeneration
Schwann cells

ABSTRACT

Shortness of donor nerves has led to the development of nerve conduits that connect sectioned peripheral nerve stumps and help to prevent the formation of neuromas. Often, the standard diameters of these devices cannot be adapted at the time of surgery to the diameter of the nerve injured. In this work, scaffolds were developed to form filled nerve conduits with an inner matrix with unidirectional channels covered by a multidirectional pore zone. Collagen type I dispersions (5 mg/g and 8 mg/g) were sequentially frozen using different methods to obtain six laminar scaffolds (P1 to P5) formed by a unidirectional (U) pore/channel zone adjacent to a multidirectional (M) pore zone. The physicochemical and microstructural properties of the scaffolds were determined and compared, as well as their biodegradability, residual glutaraldehyde and cytocompatibility. Also, the Young's modulus of the conduits made by rolling up the bizonal scaffolds from the unidirectional to the multidirectional zone was determined. Based on these comparisons, the proliferation and differentiation of hASC were assessed only in the P3 scaffolds. The cells adhered, aligned in the same direction as the unidirectional porous fibers, proliferated, and differentiated into Schwann-like cells. Adjustable conduits made with the P3 scaffold were implanted in rats 10 mm sciatic nerve lesions to compare their performance with that of autologous sciatic nerve grafted lesions. The *in vivo* results demonstrated that the tested conduit can be adapted to the diameter of the nerve stumps to guide their growth and promote their regeneration.

1. Introduction

Each year, more than one million people worldwide are affected by injuries of peripheral nerves [1]. These injuries result in functional limitations and neuropathic impacts that disturb the life quality of the patients and increase costs in the health system [2–4]. Complete transection of axon and connective tissue – neurotmesis- and damage of the axons in which the continuity of connective tissue and nerve is maintained - severe axonotmesis – are treated surgically [4]. When the size of the injury allows it, reconstructive surgical procedures like tension free end-to-end (ETE) and end-to-side (ETS) neurorrhaphies [5,6] are commonly used. The ETE procedure sutures the resulting stumps of a transected nerve, and the ETS procedure coaptates the distal stump of an injured nerve to an adjacent intact nerve [5,6]. Tension-free sutures cannot be achieved when a critical length is reached [7]. Beyond this length, sensory nerve autograft is the gold standard method to reconstruct motor sectioned nerves. In humans, gaps up to 3 cm are bridged with sensory nerve autografts [8].

* Corresponding author.
E-mail addresses: dmmillanc@unal.edu.co (D. Millán), rajimenezcr@unal.edu.co (R.A. Jiménez), luis-nieto@javeriana.edu.co (L.E. Nieto), iypovedac@unal.edu.co (I.Y. Poveda), mtorresam@unal.edu.co (M.A. Torres), sofiamsilva@ua.pt (A.S. Silva), lfospinag@unal.edu.co (L.F. Ospina), jmano@ua.pt (J.F. Mano), mrfontanillad@unal.edu.co (M.R. Fontanilla).
[1] Both authors contributed equally to this work.

https://doi.org/10.1016/j.msec.2020.111838
Received 24 July 2020; Received in revised form 14 December 2020; Accepted 22 December 2020
Available online 30 December 2020

Commonly, nerves from the patient's hand, arm or leg (*e.g.*: antebrachial cutaneous nerve, sural nerve, dorsal cutaneous nerve, superficial peroneal nerve, and posterior and lateral cutaneous) are used to reattach severed nerves [5]. Nevertheless, some major disadvantages of autografts include the morbidity of the donor site, low availability of autologous nerve, loss of sensitivity, and mismatches of diameter between the donor and recipient nerves [9]. Further, graft success may be limited by the size of the defect, donor nerve vascularization and graft fascicular architecture, among others [10]. Hence, allografts have been developed to overcome the limitation of autologous donor nerve. However, there is only one nerve allograft that has been approved by the FDA for nerve reconstruction [11]. As a consequence, nerve guidance conduits (NGCs) made of natural, synthetic and hybrid materials have been used as artificial nerve grafts when an autograft is not feasible [12]. A majority of these conduits are tubular structures designed to enclose and connect the nerve stumps of a transected nerve [12].

Collagen type I is among the natural materials used to manufacture artificial grafts [11,13–16]. This protein is the main constituent of peripheral nerve extracellular matrix, and was the first natural polymer used to manufacture NGC for peripheral nerve regeneration [17]. Most of the collagens NGCs already approved by the US Food and Drug Administration (FDA) are hollow tubular structures, which reconnect a sectioned nerve after being sutured to the proximal and distal stumps [8,18]. Still, their lack of internal microstructure -in several cases- hinders the axonal regrowth required to promote axon reconnection of the distal nerve stump [19].

Experimental evidence indicates that the presence of an internal matrix with unidirectionally oriented fibers impacts peripheral nerve repair mechanisms [20]. For instance, poly (acrylonitrile-*co*-acrylate) conduits with internal aligned fibers improved axon regeneration compared to those made with the same material but with randomly oriented internal fibers [21]. Topographical signals from poly(ε-caprolactone) conduits aligned by electrospinning upregulated myelin-associated glycoprotein (MAG), protein zero (P0) and myelin basic protein (MBP) genes, and promoted Schwann cell maturation [22]. Also, a microtube array sheet (MTAS) with unidirectional topography oriented the migration of Schwann cells and the extension of neurites from spinal cord and dorsal root ganglion neurons [23]. Likewise, cylindrical scaffolds with unidirectional pores obtained by punching collagen type I and elastin unidirectional sponges, and placed on contact with rat dorsal root ganglia, promoted aligned migration of axons and Schwann cells [24]. Pre-clinical evaluation of the abovementioned conduits previously seeded with Schwann cells in a rat model of sciatic nerve defect that preserved the epineural tube, showed animals recovered without signs of inflammation or neuroma formation [25]. Despite the *in vitro* and preclinical data supporting the role of unidirectional fillers in promoting guided axon growth and nerve repair [21], the FDA has approved to commercialize only one conduit made with an external matrix of collagen type I, and an internal unidirectional oriented matrix made of collagen type I and chondroitin-6-sulphate [8,16]. Present NGCs perform well when they are grafted into short gaps: in humans the accepted success rates decrease when defects are larger than 3 cm [8,10]. However, regeneration is still significantly lower than that observed with autograft controls [21]. Thus, designing and evaluating new devices that promote regeneration of peripheral nerve is still required.

Existing NGCs are manufactured with fixed diameters. Hence, mismatches between the NGC diameter and the diameter of the stumps it intends to reconnect can occur. Such mismatches are disadvantageous because a difference in nerve gauge can lead to graft failure [8]. In previous works we have described the manufacturing of aligned laminar scaffolds of collagen type I [26]. Briefly, acidic dispersions of this protein were horizontally frozen and lyophilized to obtain laminar scaffolds (10 cm^2) with unidirectional pores in which cells adhered and grew aligned to the unidirectional fibers of their pores. The present work presents an absolutely new design of a laminar scaffold with two continuous zones of differently oriented pores (unidirectional and multidirectional). Since the two zones are continuous, the scaffold can be rolled-up by the surgeon from the unidirectional to the multidirectional zone, and in this way form a conduit adjusted to the diameter of the stumps of the peripheral nerve that has been sectioned. When rolled, the unidirectional and multidirectional zones of the scaffold will respectively form the inner fill and outer sheath of the conduit. The proposed scaffold with such a unique architecture and configuration represents a new generation of conduits that might impact *in vivo* peripheral nerve regeneration.

2. Materials and methods

2.1. Materials

Bovine tissue used to isolate collagen type I was purchased from San Martín packing plant (Bogotá, Colombia). Ethanol 96%, ethyl ether, sodium hydroxide, sodium chloride, acetic acid glacial, isopropyl alcohol, sodium sulfite, and glycine were provided by Merck (Germany). Dulbecco's Modified Eagle Medium (DMEM), fetal bovine serum (FBS), antibiotic-antimycotic solution (100×), MEM vitamin solution (100×), sodium pyruvate (100×) solution, trypsin, EDTA, MTT (3-(4,5-Dimethylthiazol-2-yl)-2,5-Diphenyltetrazolium Bromide), phosphate-buffered saline (PBS), StemPro™ adipogenesis differentiation kit, StemPro™ chondrogenesis differentiation kit, StemPro™ osteogenesis differentiation kit, and Hank's balanced solution were purchased from Thermo Fisher Scientific (Waltham, MA, USA). Rabbit complement (C12CC), sodium dimethyl sulfoxide (DMSO), forskolin, ninhydrin, collagenase type I, poly-L lysine, cytosine-β-arabinofuranoside hydrochloride, β-mercaptoethanol, and all-trans retinoic acid were supplied by Sigma-Aldrich Chemical Co (St. Louis, MO, USA). Recombinant heregulin β1, vybrant™ CFDA SE cell tracer, rabbit IgG polyclonal antibody S100b, recombinant platelet derived growth factor (PDGF-AA), recombinant basic fibroblast growth factor (bFGF), and Shandon™ Cryomatrix™ embedding resin were purchased from Thermo Fisher Scientific (Waltham, MA, USA). Rat anti-mouse Thy 1.2 antibody, rabbit IgG polyclonal p75NTR, PerCP/Cy5.5 anti-human CD105 antibody (cat. 323216), PE anti-human CD73 antibody (cat. 344004), PE/Cy7 anti-human CD45 antibody (cat. 368532), APC anti-human CD34 antibody (cat. 343608), and FITC anti-human CD90 antibody (cat. 328180) were supplied by BioLegend (San Diego, CA, USA). Goat anti-rabbit IgG H&L (FITC) was purchased from Abcam (cat. ab6717; Cambridge, MA, USA). Vectastain ABC HRP kit (peroxidase, standard), DAB peroxidase substrate kit SK-4100, antigen unmasking solution, and hematoxylin were acquired from Vector Laboratories (Burlingame, CA, USA).

2.2. Manufacturing collagen type I scaffolds and conduits

Bovine fascia bought in a certified packing plant was used to isolate the collagen. The tissue was washed, disinfected (2% sodium hypochlorite, 70% ethanol), and contaminant tissues removed. Clean tissue was cut in small pieces that were suspended in 0.5 M acetic acid, the suspension was centrifuged, and the supernatant removed. After neutralizing the supernatant (1 M NaOH) the precipitated collagen was isolated and dissolved in 0.1 M acetic acid. The resulting collagen was quantified by gravimetric analysis. For this, an aliquot of the collagen dispersion was dried (100 °C) and weighted. Once the amount of collagen present in the acetic acid dispersion was known, two collagen type I dispersions (5 and 8 mg/g collagen type I in 0.05 N acetic acid) were prepared and crosslinked with 0.02, 0.04, 0.06, 0.08, and 0.10% v/v glutaraldehyde to obtain five dispersions per each concentration. The resulting dispersions were named after the glutaraldehyde concentration: P1=0.02%; P2=0.04%, P3=0.06%; P4=0.08%, and P5=0.1% v/v. A non-cross-linked dispersion was included as control (NC). These dispersions were homogenized (10.000 rpm, 10 min) with an Ultra-Turrax ® (IKA Works, China) and then shaken (120 rpm) on an orbital shaker

(Thermo Fisher, USA) for 24 h, at 37 °C. Samples were centrifuged at 400 ×*g* (Thermo Fisher) for 30 min to eliminate bubbles. Non-crosslinked and cross-linked dispersions were used to produce non-crosslinked (NC) and cross-linked scaffolds (P1-P5 scaffolds, respectively).

Each scaffold was prepared in two steps to ensure the unidirectional and multidirectional orientation of the pores of each of the two zones. In the first step, the unidirectional zone was made by unidirectionally freezing the 5 mg/g collagen type I dispersion following a described methodology [26]. Briefly, the dispersion was poured into molds, which had one side covered by a metallic material that, in turn, had one end immersed in liquid nitrogen to create a temperature gradient with an axial orientation. The system described above was placed in an insulated container with enclosed air temperatures between 0 and 4 °C to avoid multidirectional freezing and to maintain the unidirectional pore orientation in the entire length of the U zone. In the second step, the 8 mg/g collagen dispersion was poured in direct contact with the unidirectional zone previously obtained, and frozen (−25 °C). The differentially frozen dispersions were lyophilized (Virtis, SP Industries, USA) to produce laminar scaffolds (10 cm^2, 3 mm thickness) with two clearly differentiated and continuous zones: one with unidirectional and the other with multidirectional pores. The resulting sheets were cut to obtain the bi-zonal scaffolds used in the different analyses. These scaffolds were dampened and rolled-up from the unidirectional (U) to the multidirectional (M) zone to form conduits (named as the scaffolds) with an inner unidirectional scaffold and an outer multidirectional wrapping.

2.3. Microstructural characterization of the scaffolds

2.3.1. Environmental scanning electron microscopy (ESEM)

Environmental scanning electron microscopy (ESEM) of transversal and longitudinal dried non-coated samples (8 mm [⌀], 2 mm [H]) was carried out with a Tescan Vega3 system (Tescan Vega 3 SB, Czech Republic). Electron micrographs were used to qualitatively assess the interconnectivity and directionality of scaffolds' unidirectional (U), multidirectional (M), and interface (I) zones. For these analyses, three aleatory sections per scaffold were evaluated at 45× and 150× magnification [26].

2.3.2. Pore size and porosity

Cross-sections (100 μm) of U and M zones of NC and P1-P5 scaffolds were cut, hydrated with 1× PBS, and degassed to be observed under an inverted microscope (Eclipse TS100, Nikon, Japan). Digital images were captured with the NIS-Elements AR (Ver 4.50 Nikon) software, and images were analyzed using the software ImageJ 1.39u (Wayne Rasband, NIH, USA) to evaluate pore size. The major and minor axes of the ellipse that best fitted each pore were measured and their average was used to calculate the mean pore size. A total of 60 pores chosen randomly were measured for each analysis. The obtained average values were multiplied by 1.5 to take into account the effects of the pores that were not sectioned through their maximal cross-section.

A modified liquid displacement method [27] was used to assess scaffolds porosity. Briefly, samples (2 cm^2) of U and M zones of NC and P1-P5 scaffolds were cut and weighted (W_1), immersed into 1× PBS (2 mL), degassed under vacuum (10 min), and incubated (37 °C, 24 h). Thereafter, samples were placed on a filter paper to remove the excess of PBS and weighed (W_2). A dry pycnometer was weighed (W_3), and the analyzed U or M sample placed into it. The pycnometer was filled with PBS until its volume (25 mL) was completed and weighed (W_4). Assays were carried out five times. The total porosity was measured using the aforementioned weights (W_1, W_2, W_3, and W_4) and the density (ρ) of PBS (1.023 g/mL) according with the following equation: $P\ (\%) = 1 - (\rho_{wet\ scaffold} / \rho_{collagen\ fibers}) \times 100$ [28].

2.4. Physicochemical characterization

2.4.1. Fourier transform infrared spectroscopy (FTIR)

The U and M zones of P1-P5 scaffolds were analyzed by FTIR. Each dried sample (2 mg) was mixed with KBr (200 mg) and compressed to obtain a pellet. The system was purged with dry air (1 h) to remove water vapor from the sample compartment. Spectra were obtained using a FT/IR-4200 spectrophotometer (Jasco, Germany), in a range of 4000–500 cm^{-1} with a resolution of 8 cm^{-1} and 150 scans/sample. The collagen type I used to manufacture the scaffolds was used as a control. Experiments were performed in triplicate.

2.4.2. Cross-linking degree, residual glutaraldehyde, and degradation

Scaffolds' cross-linking degree was related to the free amino groups of each sample, and assessed using the ninhydrin assay [29]. This assay is a destructive test of the samples, in which the free amino groups of the collagen are condensed with the hydroxyl groups of the reagent solution (containing 2,2-dihydroxyindane-1,3-dione) to form Schiff bases. A standard work solution (SWS) was made by mixing (1:1) solution A (4.2 g citric acid and 1.6 g sodium hydroxide in 100 mL of type I water) and solution B (4 g ninhydrin in 100 mL ethylene glycol). Then, U and M samples (1 cm^2) were covered with 500 μL of the SWS, heated (100 °C, 30 min), cooled to reach room temperature, and centrifuged (800 ×*g*, 5 min). The pellet was discarded, and the supernatant was mixed with 50% (v/v) isopropyl alcohol (1 mL). The absorbance of the samples was measured at 560 nm (TRIAD Multimode Detector, Dynex, USA). Considering the amino groups of non-crosslinked (NC) scaffolds as 100%, the percentage of cross-linked amino groups was calculated as the ratio between the optical absorbance of the P1-P5 samples and that of the NC samples [26]. Each analysis was carried out in triplicate.

Samples (1 cm^2) were taken from zones U and M of P1-P5 scaffolds and used to evaluate the residual glutaraldehyde content. They were incubated (12 h, 60 °C) with 1 mL of a solution containing 1 M NaOH, 0.1 M glycine and 0.1 M Na_2SO_3, centrifuged (400 ×*g*, 5 min), and transferred (100 μL) to a 96-well culture plate. Their absorbance was read at a wavelength of 238 nm using a Dynex spectrophotometer. Data obtained was interpolated on a calibration curve previously made with known concentrations of glutaraldehyde. All experiments were carried out in triplicate.

The enzymatic degradation of scaffolds was assessed by gravimetric analysis. Samples (8 mm [⌀], 2 mm [H]) of U and M areas of the NC and P1-P5 scaffolds were weighed (Wi) and incubated (37 °C) under shaking (80 rpm) with a solution of collagenase type I (1 mL, 250UI/mL) in 1× PBS for 24 h, 3, 15 and 30 days. Collagenase was changed every 5 days during the time of the assay. After removing the supernatants, the scaffolds were lyophilized for 24 h and weighted (Wf). The degradation percentage D (%) was calculated as follows: $D\ (\%) = 1 - (Wf / Wi) \times 100$.

2.4.3. Liquid sorption capacity, swelling, contact angle, and Zeta potential

These tests were carried out with the scaffolds. Liquid sorption capacity (LSC) was evaluated gravimetrically. Samples (2 cm^2) of U and M zones of NC and P1-P5 scaffolds were weighted (Wi) and immersed in 1× PBS (pH 7.4) for 24 h at 37 °C. Then, hydrated samples were placed on Whatman paper to remove PBS excess and weighted (Wf). Experiments were carried out five times. The liquid sorption capacity was calculated as follows: $LSC\ (\%) = (Wf - Wi) / Wi \times 100$.

Swelling of the same samples used to assess LSC was calculated by measuring the scaffolds volume change after being immersed in PBS. The width, height, and length of dry U and M areas (2 cm^2) of NC and P1-P5 scaffolds were measured with a stainless hardened caliper digital (Mitutoyo, Aurora, IL, USA) to obtain the volume of dry samples (Vd). Afterward, the Vw value calculated during the porosity evaluation of the scaffolds was used to determine their swelling percentage (S%) as follows: $S\ (\%) = (Vw / Vd) * 100$.

Scaffolds' dynamic contact angle was measured using the captive

bubble method with an automated Contact Angle Goniometer (Ramé-hart Instrument Co., NJ, USA). After hydrating the U and M samples (1cm^2) of P1-P5 scaffolds in supplemented DMEM (24 h, room temperature), each sample was fixed in the holder of the device and submerged in DMEM. Then, air (6 μL) was injected beneath the sample's surface, and digital images of the forming bubble were taken. Each evaluation was repeated three times.

The electric surface potential (Zeta potential) of U and M zones of P1-P5 scaffolds was measured with a Zetasizer Nano ZS (Malvern Instruments, UK). Samples (0.2 g) were placed in 2 mL of PBS (20 mM, pH 7.4) for 12 h and homogenized with an ultra-turrax homogenizer system (IKA 3737001 T10 basic, Cole-Palmer, UK) at 3000 rpm for 10 min. Five measurements were made per scaffold (100 runs each) at 25 °C.

2.4.4. Conduits tensile properties

Scaffolds (4 cm^2) wetted in culture medium (DMEM) for 24 h were rolled from the unidirectional to the multidirectional zone to form conduits that had the unidirectional zone inside and the multidirectional zone outside. Each zone had the same area. The Young's modulus of the resulting NC (non-cross-linked control) and P1-P5 conduits was determined with a traction assay carried out in a micro material testing machine (MMT, Shimadzu), equipped with a 101 N load cell, at a speed of 1.0 mm/min until the conduits ruptured. Samples were stretched in the direction of the unidirectional pores. The Young's modulus of the conduits was calculated from the slope of the stress-strain curves. Three measurements per each sample were made.

2.5. Cytocompatibility evaluation

2.5.1. Isolation and purification of Schwann cells

Schwann cells were isolated and cultured following described protocols [30,31]. The sciatic nerves of 10–12 pup mice (2–5 days old) were dissected, cleaned, excised, and placed (40 min at 37 °C) into culture plates containing 0.25% trypsin and 0.1% collagenase type I in DMEM without Fetal Bovine Serum (FBS). The enzymatic digestion was halted by adding 40% FBS in Hank's balanced solution; the suspension was centrifuged (400 ×*g*, 10 min). The cell pellet was resuspended in DMEM supplemented with 10% (v/v) FBS, 100 IU/mL penicillin, 100 μg/mL streptomycin, and 0.5 μg/mL amphotericin B, and then poured in culture plates (35 mm diameter) pre-coated with poly-L lysine. After incubating for 24 h (5% CO_2, 37 °C), medium was replaced with DMEM supplemented with 10 μM cytosine-β-arabinofuranoside hydrochloride, cultures incubated for an additional 48 h, and medium replaced by complete DMEM supplemented with 10 nM heregulin β1 and 2 μM forskolin [31]. Complement-mediated killing was carried out to eliminate contaminating fibroblasts. For this, cultured cells were scraped, centrifuged (400 ×*g*, 10 min), resuspended in 60 μL of rat IgG anti-mouse Thy 1.2, and incubated (30 min, 37 °C). Then, rabbit serum was added and cells were incubated for an additional 60 min (37 °C). After this time, they were washed three times with PBS and cultured with DMEM supplemented with 5 ng/mL PDGF-AA, 10 ng/mL bFGF, 10 nM heregulin-β1 and 2 μM forskolin (Schwann cell induction medium) [32] until 80% of confluence was reached. Isolated cells were characterized using rabbit polyclonal IgG antibody S100b (1:50) and secondary goat anti-rabbit IgG H&L (FITC) (1:100). Positive cells in 5th or 6th passage were used in all experiments.

2.5.2. Isolation and characterization of human adipose stem cells (hASC)

Stem cells derived from human adipose tissue (hASC) were isolated from a healthy young donor lipoaspirate with signed informed consent. Primary cultures were obtained by modifying a described methodology [33]. Briefly, tissue (3 g) was incubated (1 h, 37 °C) with 10 mL of collagenase type I (2 mg/mL) in DMEM serum-free. After digestion, DMEM supplemented with 10% FBS was added, and the sample was filtered with a cell strainer (70 μm). The resulting suspension was centrifuged (300 ×*g*, 10 min), the pellet was resuspended, and cells seeded (5×10^3 cells/cm^2) in DMEM supplemented with FBS (10% v/v), penicillin (100 IU/mL), streptomycin (100 μg/mL), amphotericin B (0.5 μg/mL), and incubated (5% CO_2, 37 °C). The medium was changed every third day until culture reached 80% of confluence. For cell expansion, cultures were sub-cultured three times using the same medium.

Third passage cells were scraped (0.25% trypsin, 0.025% EDTA) and the resulting suspension centrifuged (300 ×*g*, 10 min). Samples (5×10^4 cells/mL) were taken, incubated (30 min, 4 °C in the dark) with an antibody (PerCP/Cy5.5 anti-human CD105, FITC anti-human CD90, PE anti-human CD73, PE/Cy7 anti-human CD45, APC anti-human CD34), and washed three times with 1× PBS to evaluate their cell surface protein profile (positive CD105, CD90, CD73, negative or low expression CD45 and CD34). Each sample was analyzed by FACScantoII BD flow cytometry, recording 20,000 events per sample. Adhesion to the culture plate and differentiation into adipocytes, chondrocytes and osteoblasts were also assessed. For differentiation analyses StemPro™ (adipogenesis, chondrogenesis, and osteogenesis) differentiation kits were used, following the manufacturer's specifications. Oil Red O (7–14 days); alcian blue (14 days); alkaline phosphatase (7 days) and alizarin red S (21 days) were used to confirm differentiation.

2.6. Immunohistochemical evaluation

Scaffolds seeded with primary Schwann cells (2×10^5/cm^2) and incubated for 14 days were fixed with 4% paraformaldehyde (pH 7.4; 4 °C; 24 h), washed with 1× PBS, dehydrated, and embedded in paraffin. Samples were sectioned (6 μm), deparaffined (60 °C), and rehydrated. The antigenic recovery was made using antigen unmasking solution for 30 min. Samples were incubated individually with rabbit polyclonal IgG antibody S100b (1:200), and rabbit polyclonal IgG p75NTR (1: 250) for 1 h at room temperature. Thereafter, they were washed three times and processed with Vectastain ABC kit peroxidase rabbit IgG following manufacturer's indications. Antigens were detected with DAB peroxidase substrate kit, and samples were counterstained with hematoxylin. Stained slides were observed under a light microscope (Nikon ECLIPSE 55i, Nikon, Tokyo, Japan).

2.7. Cytocompatibility evaluation

The cytocompatibility of the scaffolds was assessed by evaluating their cytotoxicity on RSC96 and primary Schwann cells and by monitoring the proliferation of primary Schwann cells and primary hASC seeded in the scaffolds. The cytotoxicity of NC and P1-P5 scaffolds was evaluated following ISO 10993-5 [34]. The cell line RSC96 (ATCC® CRL2765™) and primary Schwann cells were seeded in 96-well plates (1×10^4 cells/100 μL medium) and incubated (37 °C, 5% CO_2, 24 h) in supplemented DMEM. Then, the culture medium was replaced by extraction medium (DMEM pre-incubated for 24 h with 1 cm^2 of each scaffold and sterilized by filtration) and cells incubated (37 °C, 5% CO_2, 24 h). Sterile DMEM supplemented with 25% DMSO and DMEM incubated with 0.2 g/mL silicone were used as positive and negative controls, respectively. Medium was removed, 50 μL of MTT (1 mg/mL) was added and samples were incubated for 2 h (37 °C, 5% CO_2). After discarding the MTT, isopropanol (100 μL) was added, and the absorbance measured at 570 nm (TRIAD Multimode Microplate Reader).

For Schwann cell proliferation experiments, cells (2×10^5/cm^2) were seeded in the U zone of the scaffolds and incubated (5% CO_2, 37 °C) for 24 h, 7 and 14 days with DMEM (supplemented with10% (v/v) FBS, antibiotic-antimycotic, MEM vitamin solution, sodium pyruvate solution, 10 nM heregulin-β1, and 2 μM forskolin) [31]; medium was changed every three days. A vibrant® MTT kit was used where the incubation time suggested by the manufacturer was modified from 4 h to 3 h. The formazan produced was solubilized with dimethyl sulfoxide (DMSO) and the absorbance of the samples was measured at 570 nm (Dynex Technologies). Cell distribution and alignment in the scaffolds

were evaluated with a vybrant™ CFDA SE cell tracer, following the manufacturer's specifications.

For the hASC proliferation experiments cells (2.0×10^4) were seeded in the U zones of the P3 scaffolds (8 mm [∅], 2 mm [H]), which then were divided into two groups. Group I was incubated (5% CO_2, 37 °C) with DMEM supplemented with 10% FBS for 14 days changing medium every third day. Group II was incubated (5% CO_2, 37 °C) with DMEM supplemented with 1 mM β-mercaptoethanol (Schwann cell pre-induction medium) for 24 h, medium removed, cells washed with 1× PBS and incubated (5% CO_2, 37 °C) with Schwann cell induction medium [32]. The induction medium was changed every third day, and proliferation at 24 h, 7, and 14 days evaluated using the Vibrant® MTT kit.

2.8. Animal experiment

Animals used were manipulated following the ARRIVE guidelines of the National Centre for the Replacement, Refinement & Reduction of Animals in Research [35]. The protocol was approved by the Ethics Committee of the Faculty of Sciences of the Universidad Nacional de Colombia (Act 07-2015). Twenty-one male Wistar rats (12 wk.; 250 g), were randomly divided into three groups, of 7 animals. For the procedure, each animal was anesthetized (peritoneal injection of ketamine, 70 mg/kg; xylazine, 10 mg/kg) and at random a thigh was chosen, shaved, and cleaned with ethanol (70%) before making an incision in the skin without affecting muscles. Once exposed, the sciatic nerve was transected to remove a segment of 10 mm. In the first group (I) of animals, the segment of the severed nerve was inverted and reimplanted. In the second group (II), a conduit made with a P3 scaffold pre-moistened with PBS was attached to the nerve stumps with fibrin sealant (Tissel, Baxter) and sutured (ethilon 9-0 epineural round tip). In the third group (III), the sciatic nerve gap was left unbridged. A plastic surgeon and two veterinaries carried out the surgeries. Thereafter, animals were kept in individual cages with food and water *ad libitum* and tramadol (5 mg/g) was injected subcutaneously to control the animal pain. Evaluation of pain, stress, and distress produced by the surgical procedure was carried out according to published guidelines [36]. Healing was monitored by assessing the signs described in the National Research Council Guide for the Care and Use of Laboratory Animals [37]. The animals were sacrificed 12 weeks after grafting.

2.9. Walking track analysis

Following a described methodology [38], a walking track analysis was carried out at weeks 4, 8, and 12 to calculate the sciatic functional index (SFI). For each animal, the footprints of both the grafted (E) and normal (N) limbs were digitalized and measured using the ImageJ program. The distances from the heel to the tip of the third toe (print length-PL), the first to the fifth toe (toe spread-TS), and the fourth to the second toe (intermediary toe spread-ITS) were measured and the SFI was calculated according to the following equation: $SFI = -38.33((EPL - NPL) / NPL) + 109.5 ((ETS - NTS) / NTS) + 13.3 ((EITS - NITS) / NITS) - 8.8$ [38]. In these test SFI values equal to 0 and −100 correspond to non-injured and completely transected sciatic nerves, respectively.

2.10. Muscle-mass ratio and Masson's Trichrome staining

Once the animals were sacrificed, the gastrocnemius muscle of the implanted thigh and that of the non-implanted thigh were dissected and fixed (4% paraformaldehyde, 24 h) to assess the muscle-mass ratio. For this, wet muscles of injured (Wi) and healthy contralateral sides (Wh) were weighed after removing the excess of paraformaldehyde and the ratio Wi/Wh was determined [39]. For the histological evaluation of muscle atrophy, the gastrocnemius muscle fragments (5–8 mm) were dehydrated, embedded in paraffin, and processed with a microtome to obtain cross-sections (5 μm) that were stained with Masson's Trichrome. Sections were observed under the light microscope (Olympus BX51).

2.11. Axonal density, diameter and myelin sheath thickness

For the histomorphometric analysis, the nerves were fixed with glutaraldehyde (4%, 24 h) and the areas of the nerve near the distal coaptation site were transversely cut into thin sections (1 mm). The contralateral uninjured nerve served as normal control. Sections were fixed with osmium tetroxide (1%, 2 h), dehydrated, embedded in Epon resin, and the blocks processed to obtain sections of 1 μm of thickness, which were stained with 1% toluidine blue [40]. The images were captured, digitized, and analyzed with the ImageJ program to determine axonal density, axon diameter, and myelin sheath thickness. In addition, nerves randomly chosen from each group were fixed with paraformaldehyde (4%), washed, embedded in Cryomatrix, frozen, and cut lengthwise (5 μm) with a cryostat. Slides were observed under a fluorescent microscopy (100×) (Olympus BX51) at a wavelength of 495 nm to visualize the longitudinal arrangement of the fibers of the repaired axons.

2.12. Statistical analysis

Data are shown as the mean ± the standard deviation (SD). A one-way ANOVA test was used to evaluate differences between the samples, which were significant when $p < 0.05$ or $p < 0.01$.

3. Results

3.1. Macroscopic appearance of scaffolds

The macroscopic appearance and ESEM analysis of the laminar bizonal scaffolds are shown in Fig. 1. A scaffold diagram shows the general organization and pore orientation of the U, I and M regions of the roll-up sheet (Fig. 1A). The stereoscopic observation of cross-linked scaffolds confirmed the presence of U and M continuous zones, each with different pore orientations (Fig. 1B). Scaffolds were moistened with Dulbecco's Modified Eagle's Medium (DMEM) -which is red- in order for them to fold from the unidirectional to the multidirectional zone. On account of this the conduit formed with an axially oriented internal filler wrapped by the scaffolds' zone with multidirectional pores turned red (Fig. 1C). The size of a laminar scaffolds is 10 cm^2. One sheet can be cut to obtain several 1 cm^2 scaffolds with two clearly differentiated and continuous U and M zones. Once moistened, these scaffolds can be folded and adjusted according to the diameter of the nerve stumps (Fig. 1D).

3.2. Environmental scanning electron microscopy (ESEM) of scaffolds

Representative ESEM images of U and M zones of NC and P1-P5 scaffolds are shown in Fig. 2. In all cases, the longitudinal sections clearly evidenced the continuity of the U and M zones (Fig. 2A). This continuity was also observed in the cross-sections of these scaffolds (Fig. 2B). All the cross-sections of the scaffolds presented well-defined pores in their U zones, apparently, with larger size than those in the M zones. This later zone also appeared to have higher fiber density than the U zone. The enlarged view of the M zone cross-sections of all scaffolds (Fig. 2C) showed pores that were heterogeneously shaped and, apparently, with low interconnectivity. The enlarged view of the U zones showed pores with a more homogeneous shape (Fig. 2D). Continuous channels were observed in the longitudinal sections of all U zones (Fig. 2E).

3.3. Fourier transform infrared spectroscopy (FTIR)

The results of the FTIR analysis of the scaffolds are shown in Fig. 3.

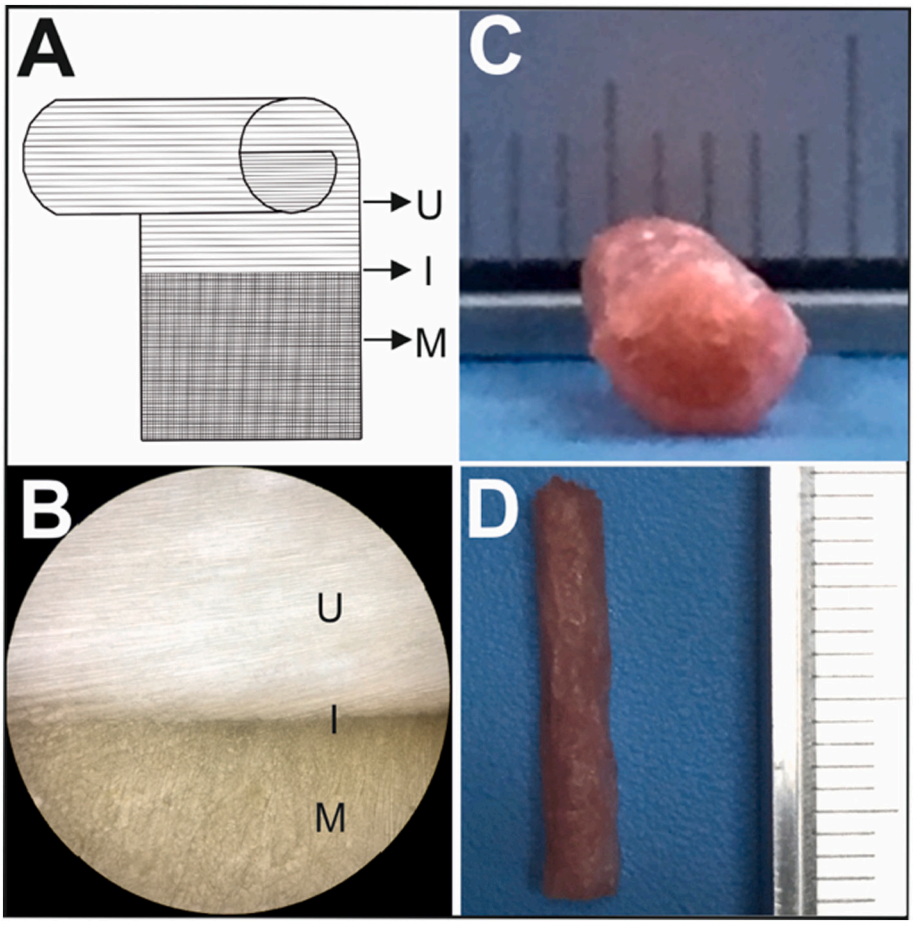

Fig. 1. Macroscopic appearance of the scaffold and conduit. (A) Diagram of the laminar roll-up scaffold. (B) Stereoscopic image of the scaffolds U and M continuous zones. (C) Cross-section of a conduit made from bi-zonal laminar scaffolds. (D) Longitudinal image of conduit. U: unidirectional zone; I: interface zone; M: multi-directional zone.

The spectra of all samples show the characteristic signals of the type I collagen included as a control (C), confirming that conduit manufacturing does not denature native collagen. The observed absorbance peaks are amide-A (N-H stretch) at 3334 cm^{-1} (M zones) and at 3307 cm^{-1} (U zones); amide-I (C=O stretch) at ≈1660 cm^{-1} (M zones) and 1654 cm^{-1} (U zones); amide-II (C-N stretch, N-H bend combination) at ≈1557 cm^{-1} (M zones) and 1551 cm^{-1} (U zones), amide-III (C-N stretch, N-H bend, C-C stretch) at ≈1239 cm^{-1} for both zones. In contrast, gelatin spectrum was different.

3.4. Pore size and porosity

Pore size data from wet scaffolds (Fig. 4) indicates that the dispersion of the pore size was greater in the M zones than in the U zones, also, that there were no significant differences between the pore size of both zones (Fig. 4A, B). The value range for the M zones was 100–500 μm with an average of 286.6 ± 129 μm, while the range for the U zone was 100–400 μm with an average of 211.3 ± 100 μm. In addition, the differences between the mean pore size of the M and U zones were significant ($p = 0.00269 \times 10^{-6}$). The evaluation of porosity is presented in Fig. 4C. Both zones are highly porous, however, the porosity, although not significantly different, was higher in zones M (>90%) than in zones U (>80%). Moreover, porosity was not affected by the concentration of the cross-linking agent and was similar to the porosity of the NC scaffolds.

3.5. Cross-linking degree, residual glutaraldehyde, and enzymatic degradation of the scaffolds

The assessment of the free amino groups in each scaffold was used to indirectly measure their cross-linking percentage (Fig. 5A). The U zone of the P1-P3 scaffolds – made with the collagen dispersion of 5 mg/g and cross-linked with the lower concentrations of glutaraldehyde (0.02 and 0.04 v/v) - showed significantly higher ($p < 0.05$) cross-linking degree than the M zones of these scaffolds, that were made with the collagen dispersion of 8 mg/g. When 0.06, 0.08 and 0.1% glutaraldehyde was used there were no significant differences between the cross-linking percentages of the U and M zones of the scaffolds, and the cross-linking degree did not increase when glutaraldehyde concentration was increased. Comparison of the cross-linking percentages of the U zones shows that there were significant differences between NC and P1 and P2-P5 scaffolds, and no differences between P2-P5 scaffolds. When the M zones were compared there were significant differences between NC, P1, and P2 with P3-P5 scaffolds, and no differences were found between P3-P5 scaffolds.

The multidirectional P1 and P2 samples did not have residual glutaraldehyde, and the P3-P5 samples had less than 6.0×10^{-4} mg glutaraldehyde/mg scaffold. Residual cross-linker increased when glutaraldehyde increased, and the cross-linker concentration in the M zones was significantly lower ($p < 0.05$) than in the U zones for all the scaffolds (Fig. 5B). In the U zones of P1-P5 scaffolds residual glutaraldehyde increased and was higher than that observed in the M zones.

Fig. 5C and D, respectively, shows the percentage of degradation of M and U zones. Both zones of the NC scaffolds were fully degraded after

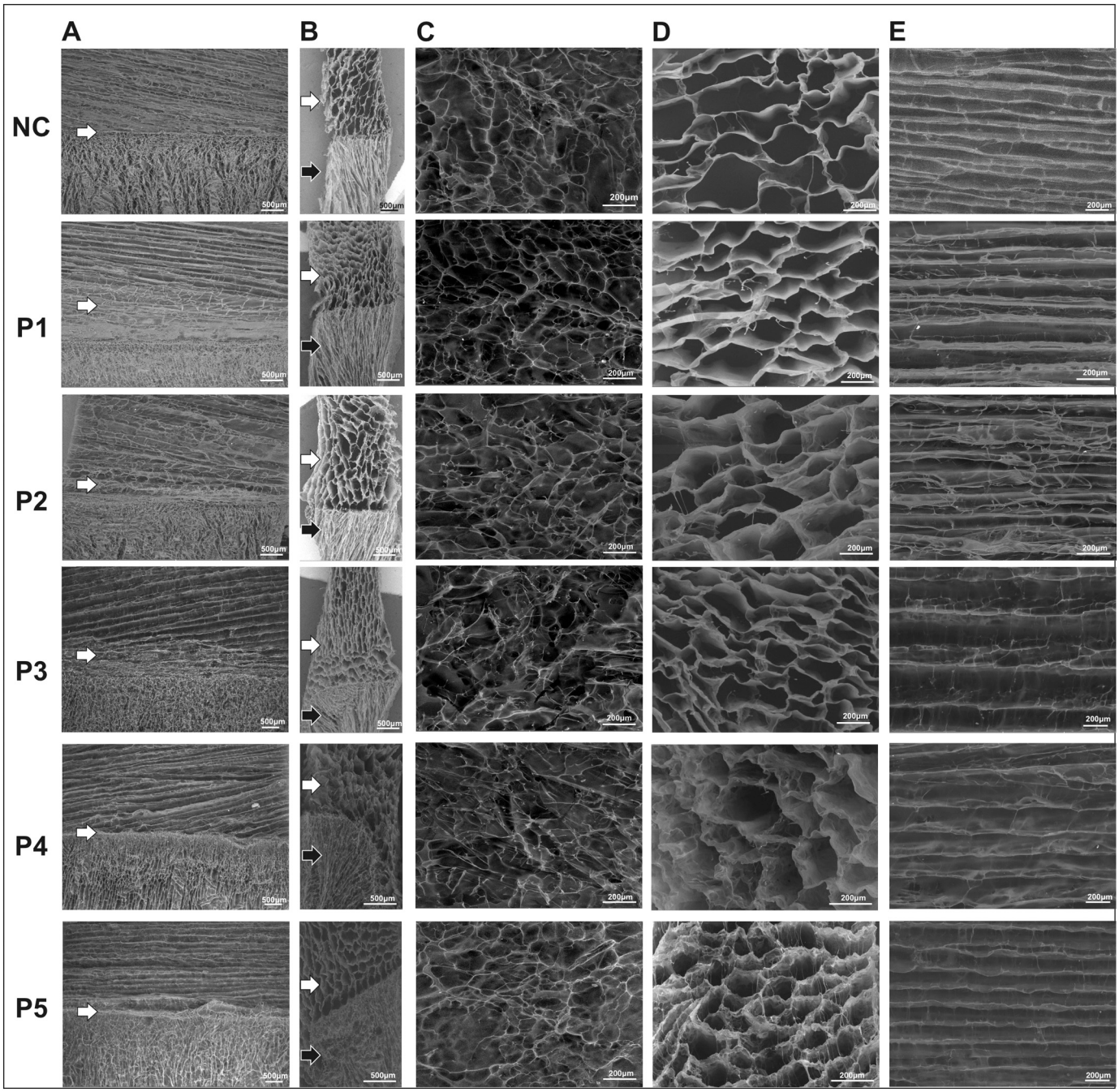

Fig. 2. ESEM evaluation of the scaffolds. Representative images of non-cross-linked (NC) and cross-linked P1-P5 scaffolds. (A) Longitudinal sections. (B) Cross-sections. (C) Enlarged cross-sections of scaffolds' M zones. (D) Enlarged cross-sections of scaffolds' U zones. (E) Enlarged longitudinal-sections of scaffolds' U zones. Arrows point the interphase between the scaffolds' U and M zones. Scale bars: 500 and 200 μm.

24 h of digestion oppositely to the cross-linked P1-P5 scaffolds. In fact, most of the M zones of the P1 scaffolds degraded completely in 30 days, while the U zones of these scaffolds did so after 14 days. Also, the degradation percentages of the M zones of the P1 scaffolds were not significantly different ($p > 0.05$) from those of the M zones of the P2 scaffolds. However, the degradation percentages of the U zones of the P1 scaffolds were significantly ($p < 0.05$) higher than those of the U zones of the P2 scaffolds. At the same time, the degradation percentage of both zones of P3-P5 scaffolds were the lowest. On day 30, the percentage of degradation of these M scaffold zones was between approximately 45% and 65%, and that of the U zones was between approximately 45% and 50%. In general, the data indicates that at 30 days the U zones of the P3-P5 scaffolds degraded less than the M zones; also, that this degradation decreased when the concentration of cross-linker increased.

3.6. Liquid sorption capacity, swelling, contact angle, and Zeta potential

Table 1 shows the liquid sorption capacity (LSC) of PBS, swelling (S), contact angle (CA), and Zeta potential of NC and P1-P5 (M and U zones) samples. The LSC was significantly higher ($p < 0.05$) for the M zones than for the U zones in all scaffolds; it was also higher for P1-P5 than for the NC scaffolds. This parameter did not vary with the concentration of glutaraldehyde used as cross-linker because there were no significant differences ($p > 0.05$) between P1-P5 scaffolds. The swelling percentage of P1-P5 scaffolds was higher, in both zones, than in those of the NC scaffolds.

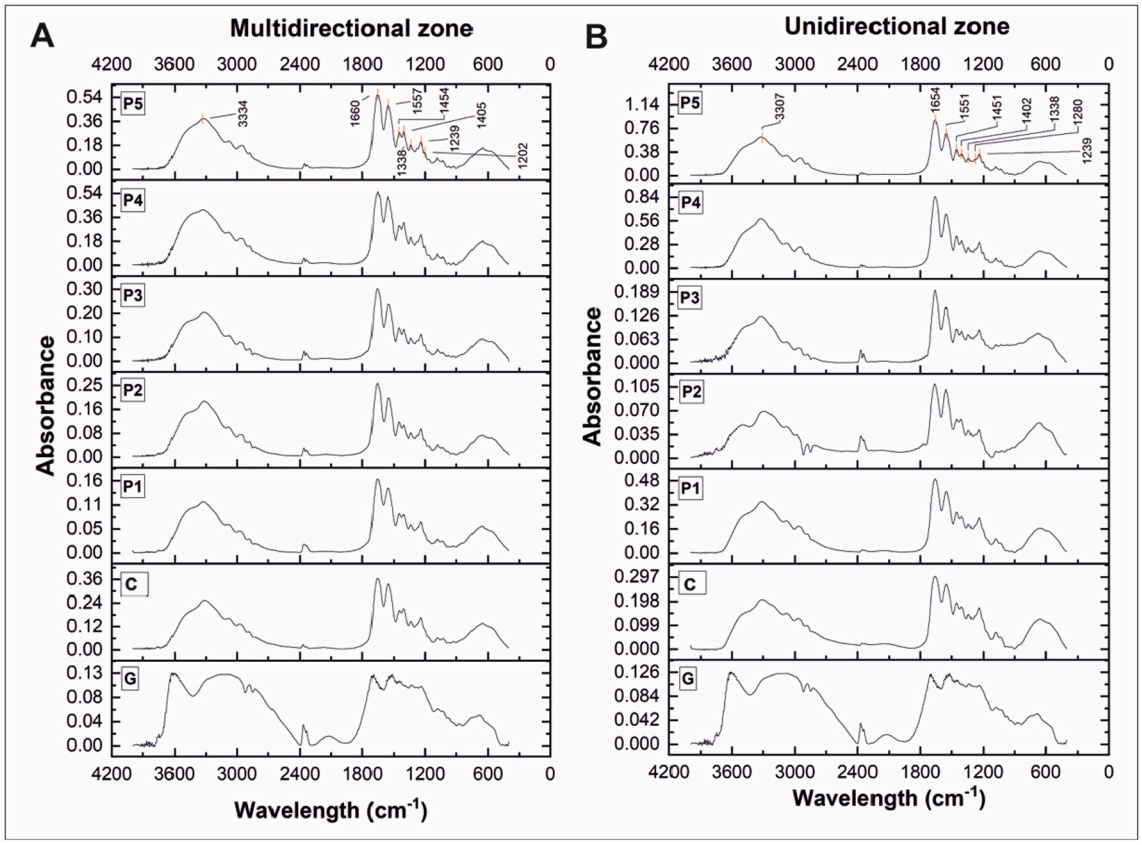

Fig. 3. FTIR analysis of the scaffolds. (A) Multidirectional zones. (B) Unidirectional zones of P1-P5 scaffolds. In both analyses collagen type I (C) and gelatin (G) were used as controls.

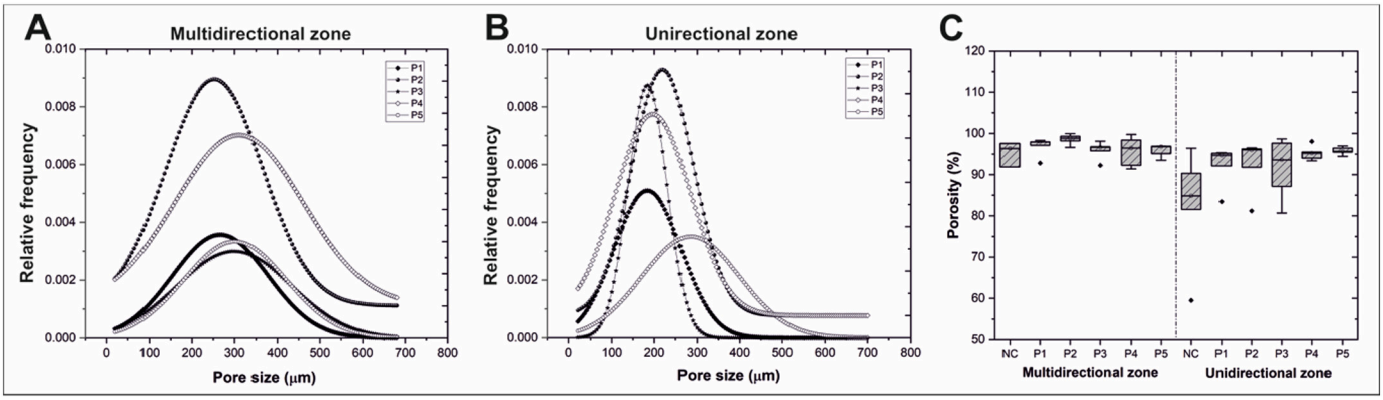

Fig. 4. Pore size distribution and porosity of the cross-linked scaffolds. (A) Pore size dispersions of the multidirectional -M- zones. (B) Pore size dispersions of the unidirectional -U- zones. (C) Porosity.

The assessment of the contact angle showed CA values above 50° and below 90° for all scaffolds, and no significant differences between M and U zones of the scaffolds. The Zeta (Z) potential of the controls, in both zones, was significantly ($p < 0.05$) higher than that of the P1-P5 scaffolds. This parameter was higher in both zones of P1samples than in those of the P2-P5 scaffolds. Negative values were only seen in the M zones of P3-P5, and there was no significant difference ($p > 0.05$) between them. In P2-P5 scaffolds, the Z potential of the M zone was significantly ($p < 0.05$) lower than that of the U zone.

3.7. Tensile properties of the conduits

The evaluation of tensile stress-strain experiments (Fig. 6) indicated that Young's modulus of the conduits prepared with the P1-P5 scaffolds increased when the concentration of the glutaraldehyde used as cross-linker increased. The Young's modulus values found were 0.027, 0.064, 0.230, 0.437, 0.876 and 0.983 MPa, respectively. Young's modulus of conduits made with NC, P1, and P2 scaffolds was not significantly different; however, conduits made with scaffolds P3, P4, and P5 had higher ($p < 0.05$) Young's modulus than the NC control.

3.8. Microscopic and immunohistochemical evaluation of Schwann cell cultures

A representative image of primary Schwann cell cultures shows spindle-shaped cells, mostly with small bodies (Fig. 7A). Moreover,

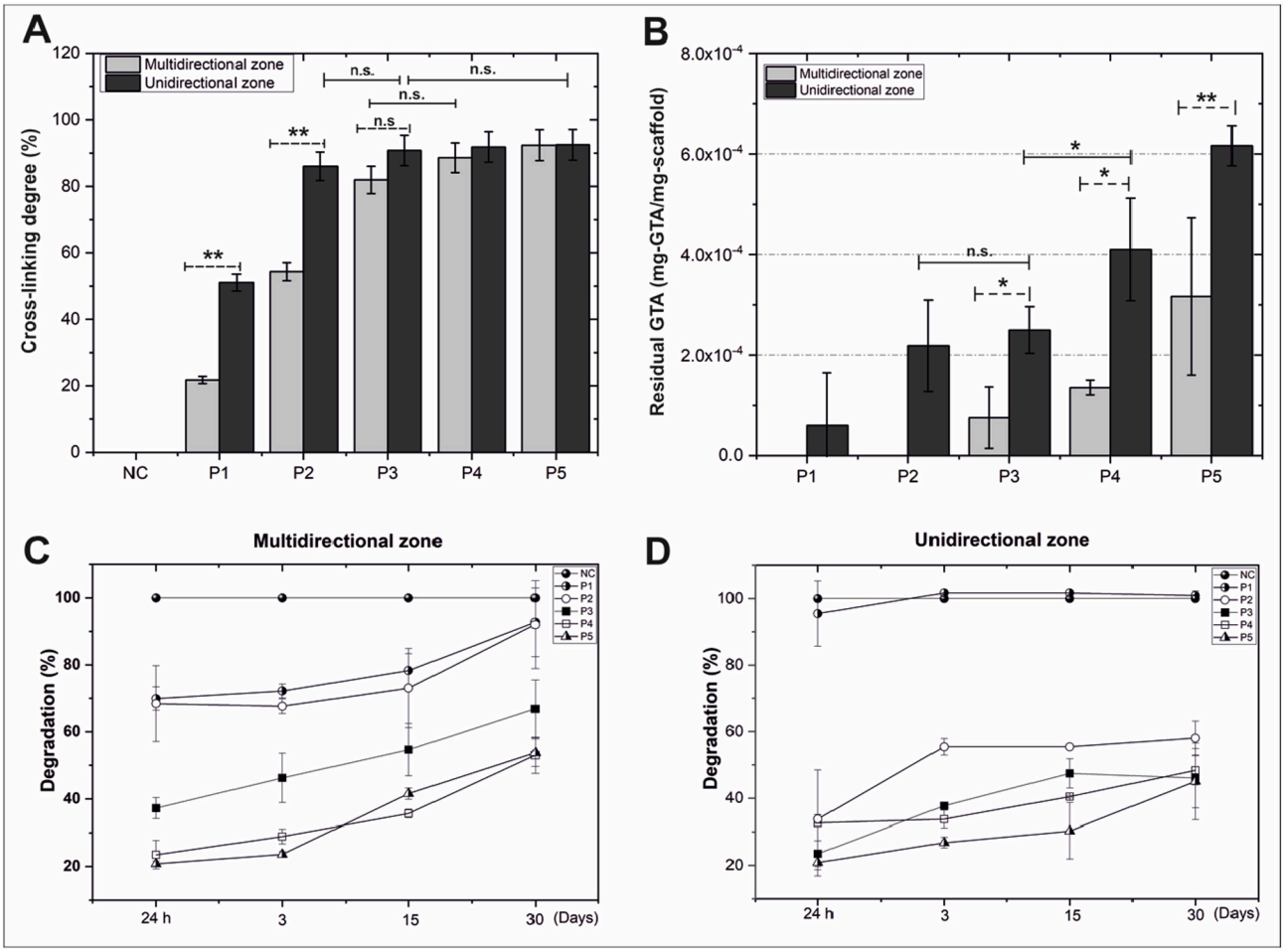

Fig. 5. Assessment of cross-linking percentage, residual glutaraldehyde, and percentage of degradation of the scaffolds. (A) Cross-linking percentage. (B) Residual glutaraldehyde. (C) Degradation percentage of NC (non-cross-linked), and cross-linked (P1-P5) scaffolds. Significant differences: *p<0.05; **p<0.01; ns.: p>0.05.

Table 1
Liquid sorption capacity, swelling, contact angle, and Zeta potential.

	NC	P1	P2	P3	P4	P5
Multidirectional zone						
Liquid sorption capacity (%)*	2288.2±433.3	5803.6±210.1	5662.2±340.0	5184.9±200.1	5688.3±118.9	5035.0±213.0
Swelling (%)*	39.9±9.9	108.0±5.1	115.6±10.0	109.1±9.6	103.8±3.7	108.18±16.85
Contact angle	63.9±4.8	53.4±0.9	62.3±9.6	76.5±6.6	70.04±6.3	72.30±7.9
Z potential (mV)	9.5±1.0	7.0±1.9	0.8±2.0	−0.8±1.0	−0.1±1.2	−1.3±1.6
Unidirectional zone						
Liquid sorption capacity (%)*	20.3±4.3	56.0±5.6	62.1±5.2	60.9±4.9	61.8±5.8	60.1±7.9
Swelling (%)*	31.2±8.2	94.2±12.0	111.3±11.1	96.5±11.6	115.1±10.1	99.1±7.9
Contact angle	62.9±9.1	50.0±9.2	76.58±12.16	73.3±9.7	81.7±8.6	72.3±6.8
Z potential (mV)	9.8±0.3	8.3±0.7	1.3±2.0	1.1±1.0	3.8±1.2	1.3±0.6

* There were no significant differences (p > 0.05) between M zones of P1to P5 scaffolds and between the U zones of these scaffolds.

immunolabelled cultures confirm the presence of spindle-shaped cells S100b positive (Fig. 7B). The *in vitro* tracing of cells labeled with carboxyfluorescein diacetate succinimidyl ester (CFDA) seeded in the U zone of P1-P5 scaffolds confirmed the adhered cells were aligned with the unidirectional collagen type I fibers. Immunolabelling demonstrated the seeded cells were S100b and p75 positive, and their adhesion to fibers of the unidirectional zones of the scaffolds (Fig. 7C).

3.9. Isolation and differentiation of human adipose stem cells

Inverted microscope analysis of isolated hASC incubated with DMEM demonstrated the presence of fusiform and polygon shaped cells adhered to the culture plate, osteogenic differentiation and cell differentiation to adipocytes, chondrocytes. The immunophenotype measured by flow cytometry showed that only 2.5% and 5.1% of cells were positive for CD 34 and CD45, respectively. Also, that 99.8%; 99.1%; and 71.8% of the isolated cells were positive for CD73, CD90, and CD105, respectively (Supplementary material, Fig. 1).

3.10. Evaluation of cytocompatibility

The cytocompatibility of the scaffolds was assessed by evaluating

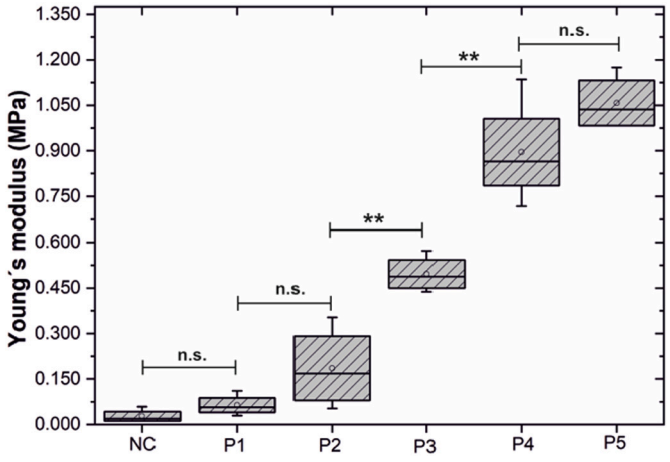

Fig. 6. Young's modulus of the conduits prepared with the cross-linked scaffolds (P1-P5) obtained from tensile experiments. Significant differences: **p<0.01; n.s.: p>0.05.

their cytotoxicity on RSC96 and primary Schwann cells, and by measuring the proliferation of primary Schwann cells and hASCs in the scaffolds (Fig. 8). The RSC96 cells - incubated with extracts from a negative control (silicone) and all the scaffolds - showed viability percentages higher than 70% of the blank viability (RSC96 cells cultured with supplemented DMEM). On the contrary, the viability was below 8% when they were incubated with the positive control extract (DMSO) (Fig. 8A). Primary Schwann cells incubated with negative control and NC and P1-P3 extracts showed viability percentages above 70%; however, when incubated with positive control and P4 and P5 extracts, they had viability percentages below 60% (Fig. 8B).

The proliferation of primary Schwann cells in the U zone of P1, P2 and P3 was significantly higher ($p < 0.05$) than in the U zone of the P4 and P5 scaffolds at 7 days. Additionally, no significant differences were found between P1, P2 and P3 ($p > 0.05$). On day 14 the number of cells in scaffolds P1, P2, and P3 were not significantly different from the number of cells counted on day 7 ($p = 0.078$; $p = 0.69$; $p = 0.58$, respectively). However, it was significantly different from day 7 in the P4 and P5 scaffolds (Fig. 8C).

The proliferation of primary hASCs, with or without the Schwann cell induction medium, was only assessed in the P3 scaffold because it was the only one that was partially degraded at 30 days and at the same time it was cytocompatible with the RSC96 cell line and primary Schwann cells. The proliferation of primary hASCs seeded in the U zone of the P3 scaffolds was significantly higher ($p < 0.05$) with the Schwann cell induction medium than that observed without it. The number of hASCs increased significantly ($p = 1.9 \times 10^{-6}$) on day 14 compared to day 7 of culture with the induction medium, and on day 7 compared to day 3 in the cultures made without it (Fig. 8D). The hASCs cultured with or without Schwann induction medium and stained with DAPI and S100b antibody are shown in Fig. 8E. The hASCs cultured in DMEM were S100b negative, while those cultured in the Schwann induction medium were S100b positive. Furthermore, cells appeared aligned along the unidirectional collagen fibers of the P3 scaffold.

3.11. Animal experiment

Animal footprints and surgical images of the healthy sciatic nerve, autograft, P3 grafted nerve, and sectioned sciatic nerve - the day of surgery and after 12 weeks - are shown in Fig. 9. This figure also presents microscopic images of the repaired nerves and the gastrocnemius muscle. The footprints of the control (Fig. 9A), autograft (Fig. 9B), P3 conduit-grafted (Fig. 9C) and non-grafted (Fig. 9D) animals indicate that all, except the controls, had flexion and toe contracture and that this contracture was more noticeable in the non-grafted rats. Although animals grafted with the P3 conduit did not fully extended the toe, they showed less contracture and an increase in toe extension similar to that seen in the autograft group at 8 and 12 weeks after surgery.

Images were taken before and after implantation to follow the appearance of the sciatic nerve. Fig. 9E shows a sciatic nerve before surgery. Images of the sciatic nerves bridged with the autograft (Fig. 9F), the P3 conduit (Fig. 9G), and non-grafted (9H) were captured during the surgeries. Twelve weeks later, when the experiment was concluded, the autograft coapted the stumps of the transected nerve (Fig. 9I), and in the animals grafted with the P3 conduit it was remodeled and replaced with nerve tissue similar in diameter to the distal stump and autologous grafted nerve (Fig. 9J). As expected, disorganized neural sprouts that did not reach the distal stump were observed in the non-grafted rats (Fig. 9K).

The histological analysis of the dissected nerves showed uniform myelinated axons with large diameters in the healthy nerve used as a control (Fig. 9L). In the autograft (Fig. 9M) and in the nerve grafted with the P3 conduit (Fig. 9N) myelinated axons of medium and small diameter were seen, grouped in small bundles and distributed along the cross-section of the nerve. However, in P3-grafted nerve, the asymmetry of the

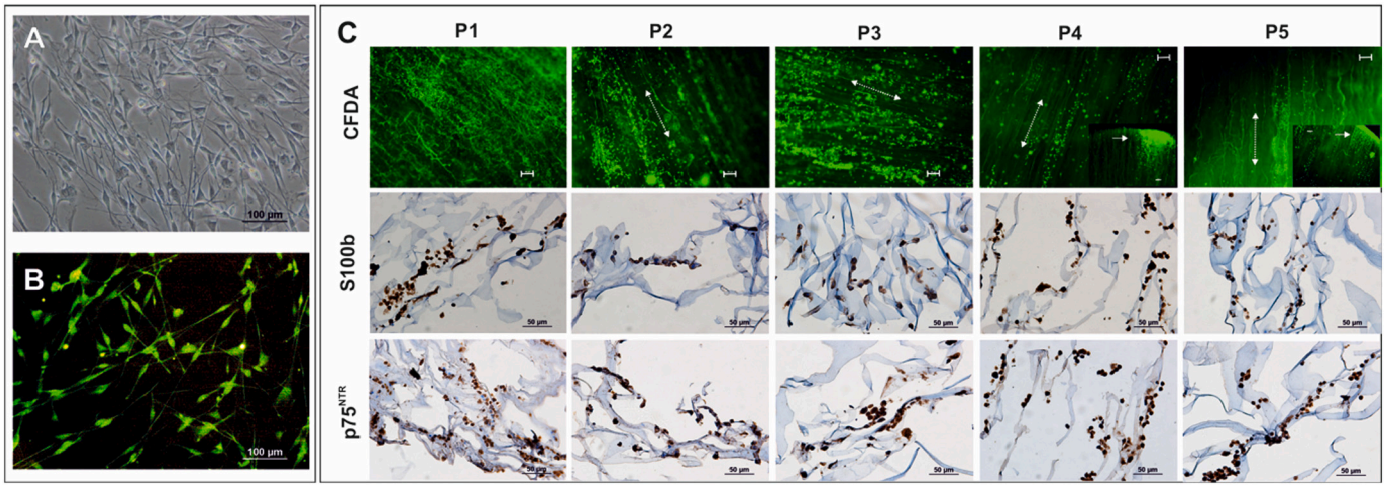

Fig. 7. Microscopic and immunohistochemical evaluation of Schwann cell cultures. (A) Primary Schwann cells. (B) Culture of Schwann cells S100b immunolabelled. (C) Schwann cells seeded in the unidirectional (U) zone of cross-linked scaffolds stained with vybrant™ CFDA, and immunolabelled with anti-S100b and $p75^{NTR}$ antibodies. Dashed arrows point oriented pore/channels. Scale bars: 50 and 100 µm.

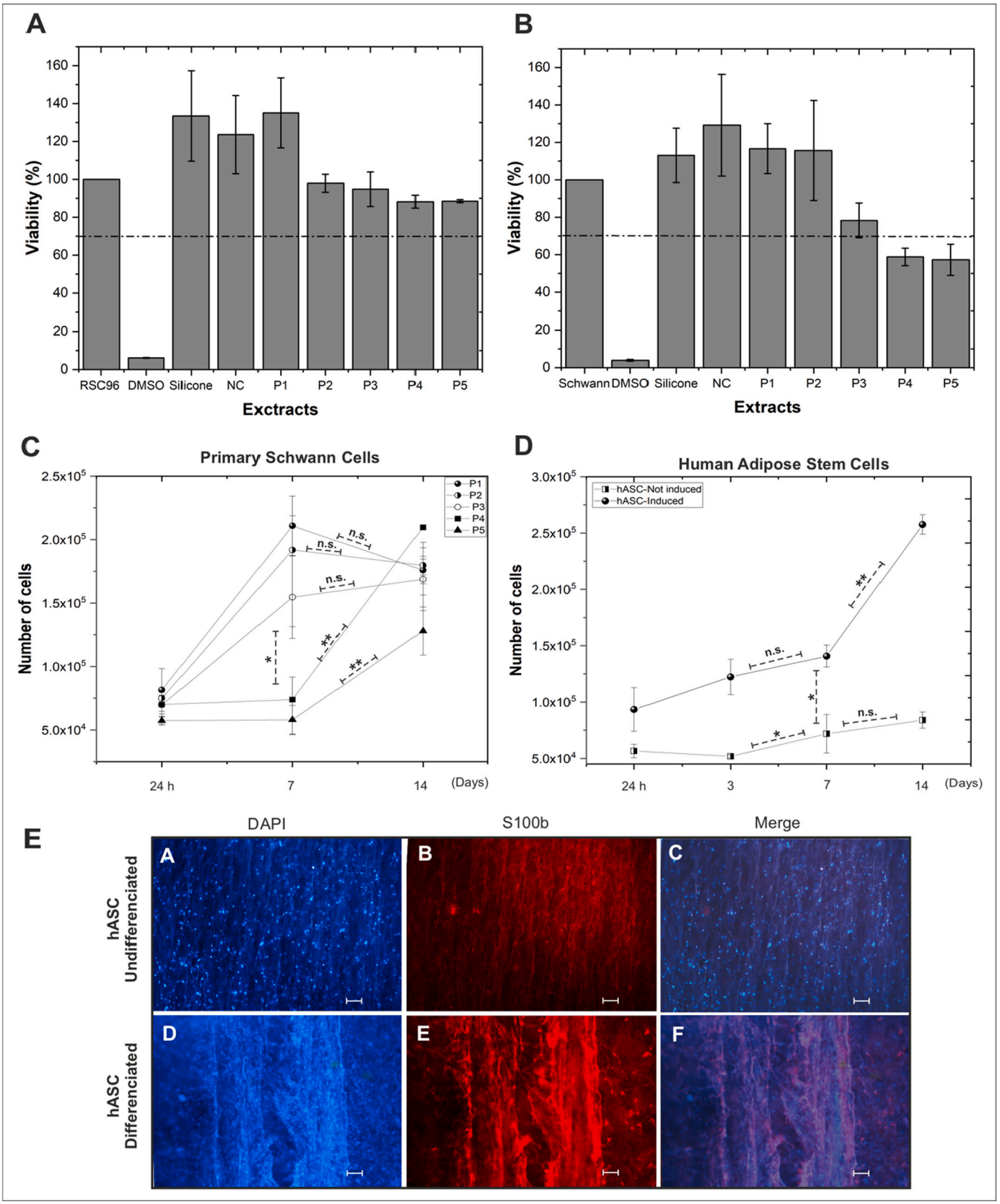

Fig. 8. Evaluation of scaffolds cytocompatibility, primary Schwann and hASC proliferation, and hASC differentiation. (A) Percentage viability of RSC96 cells. (B) Percentage viability of primary Schwann cells. (C) Primary Schwann cell proliferation in cross-linked scaffolds (P1-P5). (D) Primary hASC proliferation in the cross-linked P3 scaffold with or without Schwann induction medium. (E) Primary hASC cultured in the P3 scaffold with or without Schwann induction medium and stained with DAPI and S100b antibody. Scale bars: 100 μm.

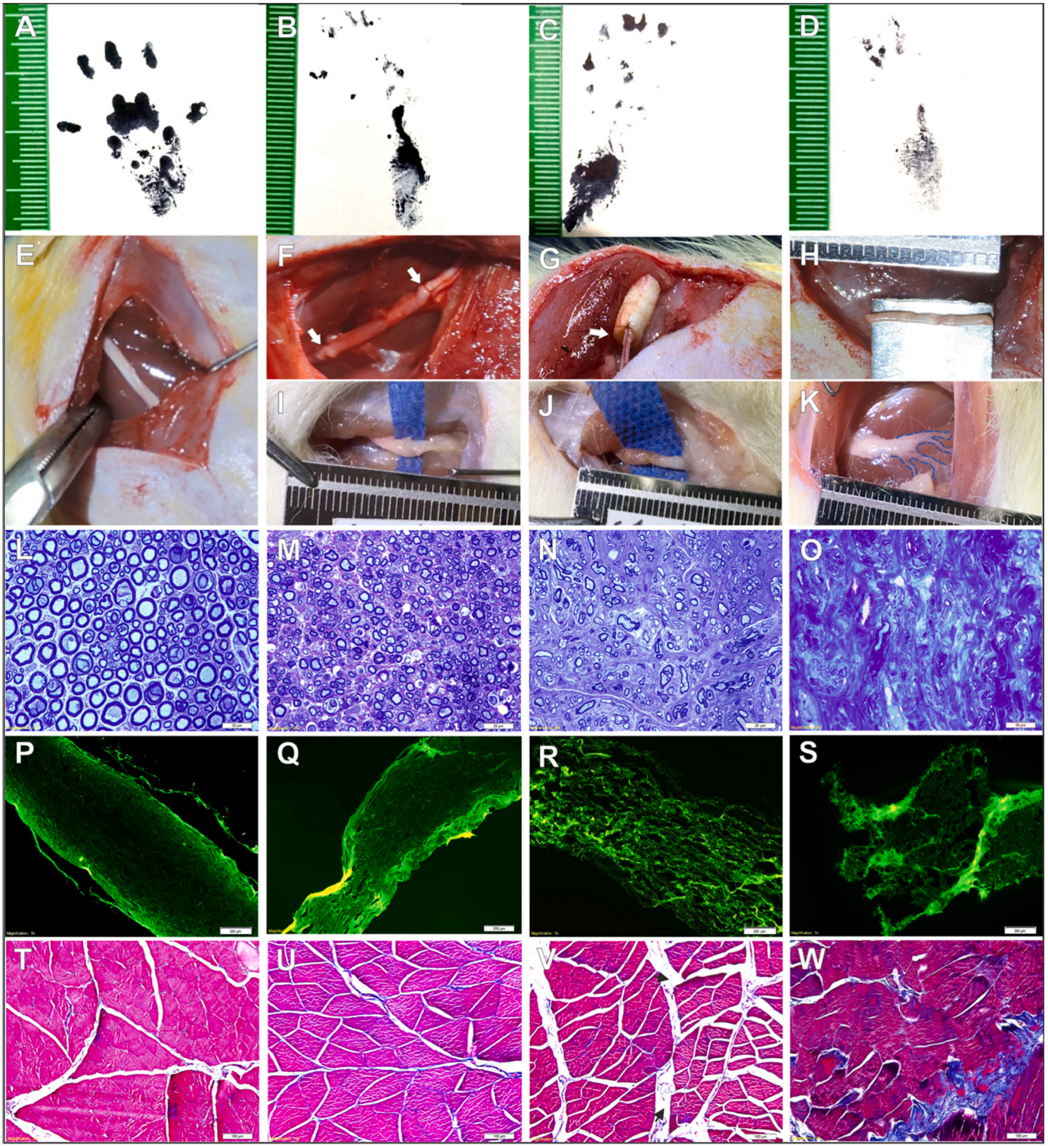

Fig. 9. Footprints, surgical and post-surgical images, and microscopic images of the repaired nerves and the gastrocnemius. Footprint of (A) Healthy, (B) Autograft implanted, (C) P3-grafted, and (D) Non-grafted animals. Surgical images of (E) Healthy sciatic, (F) Autograft implanted, (G) P3-grafted, and (H) Transected sciatic nerves. Images 12-week post-surgery of (I) Autograft, (J) P3-grafted, and (K) Non-grafted nerves. Cross-sections of (L) Healthy, (M) Autograft, (N) P3-grafted, and (O) Non-grafted nerves stained with toluidine blue. Autofluorescence images of nerve fiber fascicles from: (P) Healthy, (Q) Autograft, (R) P3-grafted, and (S) Non-grafted nerves. Histological analysis of gastrocnemius muscle from: (T) Healthy, (U) Autograft implanted, (V) P3-grafted, and (W) Non-grafted animals. White arrows on (F) points the coaptation sites. Scale Bar (L-O images: 20 μm; P-S images: 200 μm; T-W images: 100 μm). (For interpretation of the references to colour in this figure legend, the reader is referred to the web version of this article.)

axons was higher than in the autografted nerve. Few axons, abundant connective tissue, and absence of bundles were observed in the non-grafted sectioned nerve (Fig. 9O).

Longitudinal images of nerve fiber fascicles, visualized by auto-fluorescence, showed unidirectionally oriented nerve fibers in the healthy nerve (Fig. 9P) and in the nerve that received the autograft (Fig. 9Q). In the nerve grafted with the P3 conduit, the fibers were also oriented unidirectionally, however, their density was lower than in the previous cases (Fig. 9R). In the non-grafted injured nerve, the fibers were not organized (Fig. 9S). Cross-sections of the gastrocnemius muscle stained with Masson's trichrome show the characteristic polygonal shapes of healthy muscle (Fig. 9T). These polygonal shapes are also observed in the muscle of the animals implanted with the autograft (Fig. 9U) and with the P3 conduit (Fig. 9V), however, in these groups muscle has been replaced by collagen (blue stain) and adipose tissue (septate white space). In the non-grafted group, atrophic muscle fibers with irregular appearance, fibrous connective tissue and blood vessels are observed (Fig. 9W).

The sciatic functional index (SFI) was calculated to quantitatively assess the recovery of locomotor movement (Fig. 10A). The SFI was not determined in the first two weeks because the animals could not extend their toes. The SFI values at 4 and 8 weeks were significantly lower ($p < 0.05$) for the non-grafted animals than for the autografted and P3 grafted animals, and no significant differences were observed between these last two groups ($p = 0.618$). At week 12, a partial recovery of locomotor function was observed in the two grafted groups, which was not significantly different ($p = 0.999$). Most of non-grafted animals performed autotomy on two or more fingers at week 12. For that reason, the SFI of this group was not determined after week 8.

As a result of denervation of target muscles sciatic nerve injury can lead to muscle atrophy. After weighting the wet muscles of the injured (Wi) and healthy (Wh) sides the ratio Wi/Wh was determined. The animals implanted with the autograft had a higher ratio than the animals grafted with P3, however, the difference was not significant ($p = 0.083$). In the non-grafted animals, this ratio was significantly lower than in the animals that received the autograph ($p = 0.003$) and in the animals grafted with P3 ($p = 0.031$) (Fig. 10B).

The histomorphometric analysis showed similar axonal density in the healthy and grafted animals ($p > 0.05$). There were no significant differences between the autograft and P3 conduit grafted animals ($p = 0.999$). In the non-grafted group, this parameter was significantly lower than in the autograft ($p = 0.018$) and P3 conduit ($p = 0.020$) implanted groups. The diameter of the axons in the two grafted groups was similar ($p = 0.283$), however, autograft and P3 nerves diameters were significantly lower than those of the healthy control ($p = 0.004$ and $p = 1.2 \times 10^{-4}$, respectively). This parameter was significantly lower in non-grafted animals than in the autograft ($p = 0.006$) or P3 conduit grafted ($p = 0.001$) animals. Myelin thickness was similar in healthy, autograft ($p = 0.709$), and P3 grafted ($p = 0.059$) animals, and there were no differences between both grafted groups ($p = 0.432$). However, it was significantly lower in the non-grafted than in the healthy ($p = 5.2 \times 10^{-4}$), autograft ($p = 0.007$), and P3 grafted ($p = 0.001$) animals.

4. Discussion

The regeneration of peripheral nerve injuries continues to be a challenge for clinicians and researchers. Nerve autografts have been the gold standard treatment for large injures [10,41]. This approach is limited by the availability of autologous nerves, because autografts are not always successful and may result in loss of sensitivity and motor function. Different conduits have been developed to guide axonal cone growth in the injured peripheral nerves that, as a result of the size of the lesion, cannot regenerate spontaneously. Although most of these conduits work in nerve defects smaller than 3.0 cm, their use in longer injuries is controversial [8,10]. For that reason, research on new devices that promote guided regeneration of peripheral nerve is still required.

Scaffolds with oriented microstructure impact morphology and behavior of the cells that grow within them [21,42]. Previous works reported on the production of cylindrical collagen nerve guides with longitudinal channels that promote directed axonal growth [24,25].

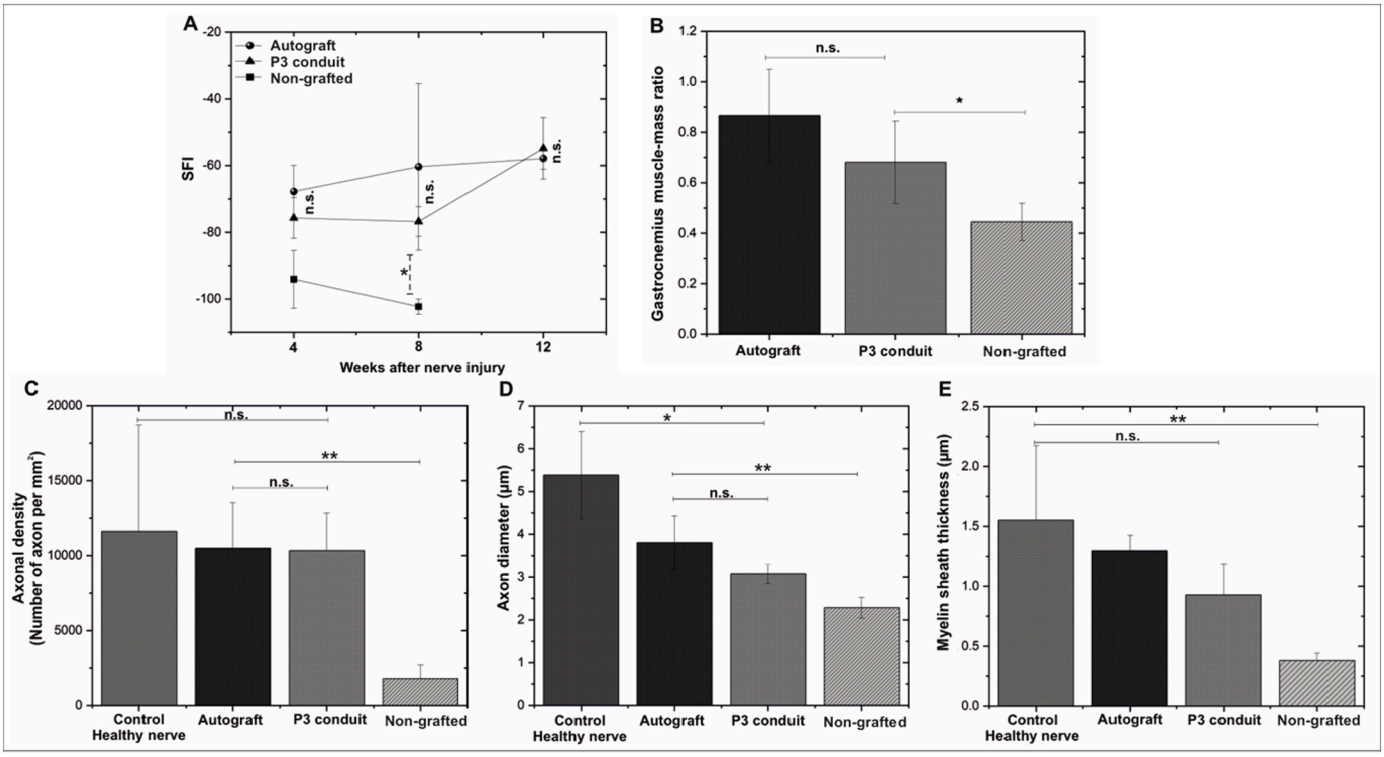

Fig. 10. Sciatic Functional Index (SFI), gastrocnemius muscle-mass ratio, and histomorphometric analysis of control, autologous grafted, P3 grafted, and non-grafted nerves. Significant differences: *p<0.05; **p<0.01; n.s.: p>0.05.

These guides were prepared using a patented unidirectional freezing procedure [43] in which a collagen dispersion containing elastin was cooled in a way that ice crystals grew in the form of finger-like structures - vertically from the bottom to the top of the cooling dispositive. The sponges with longitudinal channels obtained after lyophilization were punched to make cylinders with longitudinal oriented channels with fixed diameters and length.

In this work, 5 mg/g and 8 mg/g collagen type I dispersions were sequentially frozen using different methods to obtain laminar scaffolds (10 cm^2) formed by a unidirectional (U) pore zone adjacent to a multidirectional (M) pore zone. The scaffolds were designed to form nerve conduits filled with an inner matrix with horizontal axial channels, which is covered by the multidirectional pore zone. These nerve conduits can be adjusted to the diameter of the stumps of a sectioned peripheral nerve. The concentration of type I collagen was higher in the M zone surrounding the conduit than in its internal U zone. This was done with the intention to hinder fibroblast migration toward the unidirectional pores/channels that guide axon migration and Schwann cell adhesion and proliferation, and also to ensure mechanical protection of the intervened nerve. This novel design allows to obtain adjustable nerve conduits with a diameter that depends on the number of folds made in the unidirectional zone of the scaffold. The freezing procedure used to prepare the U zone, promoted horizontal ice crystal nucleation (under a temperature gradient). The one used to prepare the M zone promoted random ice crystal nucleation at constant temperature (−25 °C).

Six scaffold prototypes (NC, and P1-P5), non-cross-linked or cross-linked with different concentrations of glutaraldehyde, were prepared. The pores formed in the unidirectional filler were continuous throughout the entire conduit and had low interconnectivity, suggesting that they could, *in vivo*, guide axonal growth avoiding disorganized nerve sprouts. The diameter of the inner filler channels was within the range of the diameters found for individual fascicles in human femoral und upper extremity nerves (between 200 and 1000 μm) [44,45], which suggests that the space they provide *in vivo* might allow fascicles to grow and organize spatially. Although mean pore size of the M zones of all scaffolds was significantly higher than the one of the U zone, both sizes allow cell binding and diffusion of nutrients and waste material.

Gradual degradation of NGC allows guided axonal growth, while preventing the conduits from compressing the nerve that is being repaired [46]. Hence, an evaluation of the glutaraldehyde concentration needed to obtain cross-linked scaffolds that gradually degrade while sustaining the regeneration process was carried out. Non-crosslinked control and crosslinked scaffolds with the lowest concentrations (P1 and P2) were completely degraded on day 30. In contrast, scaffolds cross-linked with 0.06, 0.08, and 0.1% v/v glutaraldehyde (P3 to P5) gradually degraded not exceeding a 60% degradation after 30 days. However, residual glutaraldehyde from P4 and P5 was cytotoxic to primary Schwann cells, and cellular proliferation in these scaffolds was lower than in NC, P1, P2 and P3 scaffolds. These and the results from the cytocompatibility assay carried out to evaluate primary Schwann adhesion, proliferation and ability to preserve phenotype upon culture on the scaffolds were considered to select scaffold P3 for the assessment of hASC growth and differentiation, and to prepare the conduits used for the animal experiment.

When grafted, the conduits are exposed to biological fluids; therefore, fluid handling capacity and hydrophilicity of the scaffolds predict their ability to allow diffusion/flux of nutrients from the interstitial fluid to the surviving nervous tissue [19]. Scaffold's liquid sorption capacity depends on its chemical composition and microstructure. This work did not find significant differences in the porosity and pore size of the unidirectional and multidirectional zones of the scaffolds. However, it found that the directionality of the pore affected the liquid sorption capacity of the scaffolds. In all cases, LSC values were higher in the M than in the U zones, which might be explained by the collagen concentration used in their manufacturing. As the M zones had more collagen (8 mg/g) than the U zones (5 mg/g), they contained more hydrophilic polymeric fibers than the U zones and retained more water [26]. The network tortuosity of the M zones could also explain this result at the microstructural level. The multidirectional zones of the scaffolds might retain more liquid because they had more tortuous microstructure than the unidirectional zones [47,48]. Finally, the CA values - above 50° and below 90°- showed that all scaffolds had moderate hydrophilicity, which allows them to retain water and interact with cells [49].

The tensile properties of nerve conduits should be known because *in vivo* peripheral nerves are exposed to a tensile load that result in tensile stress [50]. Additionally, nerve conduits must be flexible to avoid compression of growing axons [12]. Young's modulus of the conduit made with the P3 scaffold (0.437 MPa) - chosen to evaluate the growth of Schwann cells and the differentiation of hASC to Schwann cells-like - is similar to the ones reported for decellularized sciatic nerve of rats (0.576 ± 0.16 MPa) [51]. This suggests that conduits made with P3 scaffolds might have the flexibility and resistance required to hinder axon compression *in vivo*.

It has been demonstrated that cell adhesion, affinity and shape are modulated by negatively and positively charged matrices. A previous work has shown that fibroblast adhesion and proliferation in poly (ε-caprolactone) (PCL) scaffolds, positively and negatively charged, was significantly different because fewer fibroblasts adhered to negatively charged scaffolds than to the positively charged ones [52]. The surface electric charge of conduits filled with fluids impact their biocompatibility when grafted in an injured nerve. Dorsal ganglia neurons and Schwann cells adhere and proliferate in positively charged oligo-(poly-ethylene glycol) fumarate (OPF) hydrogels [53]. As desired, in this work the Z potential was negative in the M zones and positive in the U zones of the P3-P5 scaffolds, suggesting the outer cover formed by the M zones of these scaffolds might not favor adherence of fibroblasts, while the inner unidirectional filling formed by the U zones might promote adhesion and proliferation of Schwann cells *in vivo*.

The cytotoxicity and ability to promote cell growth *in vitro* of the scaffolds are good predictors of their security and potential to interact with the cells they intend to guide. It was clearly shown that P3 scaffolds were non-cytotoxic for both primary Schwann cells and the neuronal Schwann cell line RSC96. In the proliferation assay, we observed that the number of primary Schwann cells on day 7 was not significantly different from the number of cells counted on day 14 for P1, P2 and P3. This result suggests that the cells entered a latency period probably induced by the change of medium that took place at that time. The number of Schwann cells in P4 and P5 increased from day 7 to day 14, probably because with the change of medium the residual glutaraldehyde that remained in these scaffolds after crosslinking was washed away.

The hASCs were used to further demonstrate the cytocompatibility of P3 because they have the potential to become Schwann-like cells and express neurotrophic factors NGF, BDNF, GDNF, and NT4 in the presence of Schwann cells [54,55]. In fact, after seeding them on the P3 scaffolds and incubating with Schwann's induction medium, they adhered and grew better than without this medium. The hASC cultured with Schwann induction medium adhered (aligned in the same direction as the unidirectional pore fibers), proliferated, and differentiated into S100b positive cells with typical spindle-shaped Schwann cell morphology. Overall, these data suggest the potential of the P3 conduit to induce mesenchymal cell differentiation to Schwann cells *in vivo*.

Taking into account data from the *in vitro* evaluation of the scaffolds (NC, P1-P5) and the tensile properties of the conduits made with them, the adjustable P3 conduit was chosen to carry out the animal study. No signs of inflammation were observed in animals implanted with the autologous nerve or with the P3 conduit. Histological analysis showed tissue with many myelinated axons in the distal portion of the grafted nerves formed in all the animals of these two groups. The diameter of the axons in the autologous and P3 implanted groups appeared smaller than the one of the healthy nerve used as control, however, the

histomorphometric analysis showed no significant differences between them. Despite there were no significant differences in the axon number and the thickness of the myelin sheath, the axons formed in P3-grafted animals appeared less symmetrical than those formed in self-grafted animals, indicating that the fibers were less mature in the first group than in the second group. Overall, animal test shows that the P3 conduit is biocompatible, integrates, and remodels when grafted into the sciatic nerve injury, promoting nerve regeneration across its width.

The gastrocnemius muscle atrophies when the sciatic nerve is injured. This results in a decrease in muscle weight and in structural changes, including the formation of fibrotic connective tissue and fat, which lead to the progressive deterioration of muscle function [55]. There were no differences in the weight of the gastrocnemius muscle between the animals grafted with the autologous nerve and those grafted with the P3 conduit. However, there were significant differences between these two groups and the non-grafted animals. Overall, these results confirm that grafting the sciatic nerve lesions evaluated in this study with the P3 conduit leads to results similar to those obtained with the autograft. Finally, the area of the laminar scaffolds that we produce is 10 cm^2, so the maximum length of a conduit would be 10 cm. An animal model would have to be developed to find out the potential limitations of grafting such conduits into a nerve gap of this length and to determine whether conduits of this size are functional.

5. Conclusions

In this work, two collagen type I dispersions were cross-linked with different concentrations of glutaraldehyde and frozen. Two freezing procedures were used sequentially to obtain a dispersion with a unidirectional pore/channel zone adjacent to one with multidirectional pores. Lyophilization of the differentially frozen dispersion produced six laminar scaffold prototypes with continuous unidirectional/multidirectional pore regions. These scaffolds can be rolled-up from the unidirectional to the multidirectional zone to form a conduit with a diameter that can be adjusted to the diameter of the stumps of a sectioned peripheral nerve, by controlling the folding of its unidirectional part. Taking into account the physicochemical, microstructural, and mechanical properties of the scaffolds, as well as their biodegradability, residual glutaraldehyde and cytocompatibility, the evaluation of the proliferation and differentiation of hASC was carried out only in cells grown in P3 scaffolds with Schwann induction medium. These cells adhered, aligned in the same direction as the unidirectional pore fibers, proliferated and differentiated into Schwann-like cells. The *in vivo* evaluation of P3 conduits in a rat model of transected sciatic nerve results confirmed that the P3 conduit leads to results similar to those obtained with the autograft. Overall, the results from this work highlight the biocompatibility of the P3 conduit with the grafted sciatic nerve.

Supplementary data to this article can be found online at https://doi.org/10.1016/j.msec.2020.111838.

Funding

This work was funded by the Departamento Administrativo de Ciencia, Tecnología e Innovación de Colombia (Colciencias - now known as MinCiencias) [Grant RC 838-2015]. Mechanical characterization of scaffolds and conduits was funded by the Portuguese Foundation for Science and Technology/MCTES [project CICECO-Aveiro Institute of Materials, Grants UIDB/50011/2020 & UIDP/50011/2020]

Disclosure

Millán D., Jiménez R., and Fontanilla MR filed the patent application No IT2020/0005215 Superintendence of Industry and Commerce, Ministry of Industry, Commerce, and Tourism, Colombia. Luis E. Nieto, Ivan Y. Poveda, Maria A. Torres, Ana S. Silva, Luis F. Ospina and João F. Mano report no conflict of interest in this work.

CRediT authorship contribution statement

Millán D.: Conceptualization, Methodology, Formal analysis, Investigation, Data curation, Writing- Original draft preparation, Visualization. **Jiménez R.A.:** Conceptualization, Methodology, Formal analysis, Investigation, Data curation, Writing- Original draft preparation. **Nieto L.E:** Investigation (Surgeries). **Poveda I.Y:** Investigation. **Torres M.A:** Investigation. **Garzón-Silva A.S:** Investigation – Reviewing. **Ospina L.F:** Investigation. **Mano J.F.:** Resources, Reviewing and Editing, Funding acquisition. **Fontanilla M. R.:** Conceptualization, Methodology, Validation, Resources, Writing - Reviewing and Editing, Formal analysis, Project administration, Supervision, Funding acquisition.

Declaration of competing interest

The authors Diana Millán, Ronal Andrés Jiménez and Marta R Fontanilla declare the following financial interests/personal relationships which may be considered as potential competing interests: Millán D., Jiménez R.A., and Fontanilla M.R filed the patent application No IT2020/0005215 Superintendence of Industry and Commerce, Ministry of Industry, Commerce, and Tourism, Colombia.

Acknowledgements

The authors wish to thank Dr. Felipe Cabello for the critical reading of the manuscript, Dr. Julia Morales F. for providing language assistance, DVM Eliana Ortiz and DVM Diane Martinez for animal care, and Diego Lara Alonso for technical assistance.

References

[1] R. Rebowe, A. Rogers, T.L. Smith, Nerve repair with nerve conduits: problems, solutions, and future directions, J. Hand Microsurg. 10 (2018) 61–65, https://doi.org/10.1055/s-0038-1626687.
[2] D.M. Wojtkiewicz, J. Saunders, L. Domeshek, C.B. Novak, V. Kaskutas, S. E. Mackinnon, Social impact of peripheral nerve injuries, Hand 10 (2015) 161–167, https://doi.org/10.1007/s11552-014-9692-0.
[3] M.-R.S. Rasulić L, Savić A, Vitošević F, Samardžić M4, Živković B, Mićović M, Baščarević V, Puzović V, Joksimović B, Novakovic N, Lepić M, Iatrogenic peripheral nerve injuries—surgical treatment and outcome: 10 years' experience, World Neurosurg. 103 (2017) 841–851. doi:https://doi.org/10.1016/j.wneu.2017.04.099. Epub 2017 Apr 24.
[4] D. Grinsell, C.P. Keating, Peripheral nerve reconstruction after injury: a review of clinical and experimental therapies, Biomed. Res. Int. 2014 (2014) 1–13, https://doi.org/10.1155/2014/698256.
[5] N.F. Sachanandani, A. Pothula, T.H. Tung, Nerve gaps, Plast. Reconstr. Surg. 133 (2014) 313–319, https://doi.org/10.1097/01.prs.0000436856.55398.0f.
[6] P. Tos, S. Artiaco, I. Papalia, I. Marcoccio, S. Geuna, B. Battiston, Chapter 14 end-to-side nerve regeneration. From the laboratory bench to clinical applications, Int. Rev. Neurobiol. 87 (2009) 281–294, https://doi.org/10.1016/S0074-7742(09)87014-1.
[7] I.R.P. Sunderland, M.J. Brenner, J. Singham, S.R. Rickman, D.A. Hunter, S. E. Mackinnon, Effect of tension on nerve regeneration in rat sciatic nerve transection model, Ann. Plast. Surg. 53 (2004) 382–387, https://doi.org/10.1097/01.sap.0000125502.63302.47.
[8] S. Mobini, B.S. Spearman, C.S. Lacko, C.E. Schmidt, Recent advances in strategies for peripheral nerve tissue engineering, Curr. Opin. Biomed. Eng. 4 (2017) 134–142, https://doi.org/10.1016/j.cobme.2017.10.010.
[9] J. Isaacs, S. Mallu, W. Yan, B. Little, Consequences of oversizing: nerve-to-nerve tube diameter mismatch, J. Bone Jt. Surg. - Am. Vol. 96 (2014) 1461–1467, https://doi.org/10.2106/JBJS.M.01420.
[10] F. Stang, G. Keilhoff, H. Fansa, Biocompatibility of different nerve tubes, Materials (Basel) 2 (2009) 1480–1507, https://doi.org/10.3390/ma2041480.
[11] T. Kornfeld, P.M. Vogt, C. Radtke, Nerve grafting for peripheral nerve injuries with extended defect sizes, Wien. Med. Wochenschr. 169 (2018) 240–251, https://doi.org/10.1007/s10354-018-0675-6.
[12] S. Kehoe, X.F. Zhang, D. Boyd, FDA approved guidance conduits and wraps for peripheral nerve injury: a review of materials and efficacy, Injury 43 (2012) 553–572, https://doi.org/10.1016/j.injury.2010.12.030.
[13] J.S. Taras, S.M. Jacoby, C.J. Lincoski, Reconstruction of digital nerves with collagen conduits, J. Hand Surg. Am. 36 (2011) 1441–1446, https://doi.org/10.1016/j.jhsa.2011.06.009.
[14] M. Bąk, O. Gutlowska, E. Wagner, J. Gosk, The role of chitin and chitosan in peripheral nerve reconstruction, Polym. Med. 47 (2017) 43–47, https://doi.org/10.17219/pim/75653.

[15] F. Neubrech, S. Heider, L. Harhaus, B. Bickert, U. Kneser, T. Kremer, Chitosan nerve tube for primary repair of traumatic sensory nerve lesions of the hand without a gap: study protocol for a randomized controlled trial, Trials 17 (2016) 17–48, https://doi.org/10.1186/s13063-015-1148-5.
[16] K.J. Wangensteen, L.K. Kalliainen, Collagen tube conduits in peripheral nerve repair: a retrospective analysis, Hand 5 (2010) 273–277, https://doi.org/10.1007/s11552-009-9245-0.
[17] R. Boni, A. Ali, A. Shavandi, A.N. Clarkson, Current and novel polymeric biomaterials for neural tissue engineering, J. Biomed. Sci. 25 (2018) 1–21, https://doi.org/10.1186/s12929-018-0491-8.
[18] J. Du, H. Chen, L. Qing, X. Yang, X. Jia, Biomimetic neural scaffolds: a crucial step towards optimal peripheral nerve regeneration, Biomater. Sci. 6 (2018) 1299–1311, https://doi.org/10.1039/c8bm00260f.
[19] V. Chiono, C. Tonda-Turo, Trends in the design of nerve guidance channels in peripheral nerve tissue engineering, Prog. Neurobiol. 131 (2015) 87–104, https://doi.org/10.1016/j.pneurobio.2015.06.001.
[20] E.C. Spivey, Z.Z. Khaing, J.B. Shear, C.E. Schmidt, The fundamental role of subcellular topography in peripheral nerve repair therapies, Biomaterials 33 (2012) 4264–4276, https://doi.org/10.1016/j.biomaterials.2012.02.043.
[21] Y. tae Kim, V.K. Haftel, S. Kumar, R.V. Bellamkonda, The role of aligned polymer fiber-based constructs in the bridging of long peripheral nerve gaps, Biomaterials 29 (2008) 3117–3127, https://doi.org/10.1016/j.biomaterials.2008.03.042.
[22] C. Sing Yian, M. Ruifa, H. Ahmet, L. Kam W, The effect of the alignment of electrospun fibrous scaffolds on schwann cell maturation, Biomaterials 29 (2008) 653–661, https://doi.org/10.1016/j.biomaterials.2007.10.025.
[23] Y. Wang, W. Wang, Y. Wo, T. Gui, H. Zhu, X. Mo, C.C. Chen, Q. Li, W. Ding, Orientated guidance of peripheral nerve regeneration using conduits with a microtube array sheet (MTAS), ACS Appl. Mater. Interfaces 7 (2015) 8437–8450, https://doi.org/10.1021/acsami.5b00215.
[24] A. Bozkurt, G.A. Brook, S. Moellers, F. Lassner, B. Sellhaus, J. Weis, M. Woeltje, J. Tank, C. Beckmann, P. Fuchs, L.O. Damink, F. Schügner, I. Heschel, N. Pallua, In vitro assessment of axonal growth using dorsal root ganglia explants in a novel three-dimensional collagen matrix, Tissue Eng. 13 (2007) 2971–2979, https://doi.org/10.1089/ten.2007.0116.
[25] A. Bozkurt, F. Lassner, D. O'Dey, R. Deumens, A. Böcker, T. Schwendt, C. Janzen, C.V. Suschek, R. Tolba, E. Kobayashi, B. Sellhaus, S. Tholl, L. Eummelen, F. Schügner, L. Olde Damink, J. Weis, G.A. Brook, N. Pallua, The role of microstructured and interconnected pore channels in a collagen-based nerve guide on axonal regeneration in peripheral nerves, Biomaterials 33 (2012) 1363–1375, https://doi.org/10.1016/j.biomaterials.2011.10.069.
[26] E. Suesca, A.M.A. Dias, M.E.M. Braga, H.C. de Sousa, M.R. Fontanilla, Multifactor analysis on the effect of collagen concentration, cross-linking and fiber/pore orientation on chemical, microstructural, mechanical and biological properties of collagen type I scaffolds, Mater. Sci. Eng. C 77 (2017) 333–341, https://doi.org/10.1016/j.msec.2017.03.243.
[27] S.T. Ho, D.W. Hutmacher, A comparison of micro CT with other techniques used in the characterization of scaffolds, Biomaterials 27 (2006) 1362–1376, https://doi.org/10.1016/j.biomaterials.2005.08.035.
[28] V. Karageorgiou, D. Kaplan, Porosity of 3D biomaterial scaffolds and osteogenesis, Biomaterials 26 (2005) 5474–5491, https://doi.org/10.1016/j.biomaterials.2005.02.002.
[29] B. Starcher, A ninhydrin-based assay to quantitate the total protein content of tissue samples, Anal. Biochem. 292 (2001) 125–129, https://doi.org/10.1006/abio.2001.5050.
[30] F. Nault, P. De Koninck, Dissociated hippocampal cultures: protocols for neural cell culture, in: L.C. Doering (Ed.), Protoc. Neural Cell Cult. Springer Protoc. Handbooks, 4th ed., Humana Press, Totowa, NJ, 2010, pp. 137–159, https://doi.org/10.1007/978-1-60761-292-6.
[31] N.D. Andersen, S. Srinivas, G. Piñero, P.V. Monje, A rapid and versatile method for the isolation, purification and cryogenic storage of Schwann cells from adult rodent nerves, Sci. Rep. 6 (2016) 1–17, https://doi.org/10.1038/srep31781.
[32] M. Georgiou, J.P. Golding, A.J. Loughlin, P.J. Kingham, J.B. Phillips, Engineered neural tissue with aligned, differentiated adipose-derived stem cells promotes peripheral nerve regeneration across a critical sized defect in rat sciatic nerve, Biomaterials 37 (2015) 242–251, https://doi.org/10.1016/j.biomaterials.2014.10.009.
[33] M. Araña, M. Mazo, P. Aranda, B. Pelacho, F. Prosper, Adipose tissue-derived mesenchymal stem cells: isolation, expansion, and characterization, Methods Mol. Biol. 1036 (2013) 47–61, https://doi.org/10.1007/978-1-62703-511-8_4.
[34] ISO 10993-5, Biological evaluation of medical devices - Part 5: in vitro cytotoxicity tests, 3rd Edition, 2009, 2009-06-01, https:/www.iso.org/standard/36406.html. (Accessed 6 June 2020).
[35] C. Kilkenny, W.J. Browne, I.C. Cuthill, M. Emerson, D.G. Altman, Improving bioscience research reporting: the arrive guidelines for reporting animal research, Animals 4 (2013) 35–44, https://doi.org/10.3390/ani4010035.
[36] D.B. Morton, P.H. Griffiths, Guidelines on the recognition of pain, distress and discomfort in experimental animals and an hypothesis for assessment, Vet. Rec. 116 (1985) 431–436, https://doi.org/10.1136/vr.116.16.431.
[37] Guide for the Care and Use of Laboratory Animals, 2011, https://doi.org/10.17226/12910.
[38] L. Costa, M. Simoes, A. Mauricio, A. Varejao, International review of neurobiology, in: Elsevier (Ed.), Essays on Peripheral Nerve Repair and Regeneration, Int. Rev. Neurobiol, 2009, pp. 127–136.
[39] F. Ma, Z. Xiao, D. Meng, X. Hou, J. Zhu, J. Dai, R. Xu, Use of natural neural scaffolds consisting of engineered vascular endothelial growth factor immobilized on ordered collagen fibers filled in a collagen tube for peripheral nerve regeneration in rats, Int. J. Mol. Sci. 15 (2014) 18593–18609, https://doi.org/10.3390/ijms151018593.
[40] S.G.A. van Neerven, K. Haastert-Talini, A. Boecker, T. Schriever, C. Dabhi, K. Claeys, R. Deumens, G.A. Brook, J. Weis, N. Pallua, A. Bozkurt, Two-component collagen nerve guides support axonal regeneration in the rat peripheral nerve injury model, J. Tissue Eng. Regen. Med. 11 (2017) 3349–3361, https://doi.org/10.1002/term.2248.
[41] S. Mobini, B.S. Spearman, C.S. Lacko, C.E. Schmidt, Recent advances in strategies for peripheral nerve tissue engineering, Curr. Opin. Biomed. Eng. 4 (2017) 134–142, https://doi.org/10.1016/j.cobme.2017.10.010.
[42] S.Y. Chew, R. Mi, A. Hoke, K.W. Leong, The effect of the alignment of electrospun fibrous scaffolds on Schwann cell maturation, Biomaterials 29 (2008) 653–661, https://doi.org/10.1016/j.biomaterials.2007.10.025.
[43] U.S. Patent, Method for producing porous structures, US 6,447,701 B1, 2008. https://patentimages.storage.googleapis.com/13/7e/28/2eaffa567acc26/US6447701.pdf.
[44] K.J. Gustafson, G.C.J. Pinault, J.J. Neville, I. Syed, J.A. Davis, J. Jean-Claude, R. J. Triolo, Fascicular anatomy of human femoral nerve: implications for neural prostheses using nerve cuff electrodes, J. Rehabil. Res. Dev. 46 (2009) 973–984, https://doi.org/10.1682/JRRD.2008.08.0097.
[45] N.A. Brill, D.J. Tyler, Quantification of human upper extremity nerves and fascicular anatomy, Muscle Nerve 56 (2017) 463–471, https://doi.org/10.1002/mus.25534.
[46] W. Daly, L. Yao, D. Zeugolis, A. Windebank, A. Pandit, A biomaterials approach to peripheral nerve regeneration: bridging the peripheral nerve gap and enhancing functional recovery, J. R. Soc. Interface 9 (2012) 202–221, https://doi.org/10.1098/rsif.2011.0438.
[47] F. Ganji, S. Vasheghani-Farahani, E. Vasheghani-Farahani, Theoretical description of hydrogel swelling: a review, Iran, Polym. J. (English Ed. 19) (2010) 375–398.
[48] H.-I. Chang, Y. Wang, Cell responses to surface and architecture of tissue engineering scaffolds, in: Regen. Med. Tissue Eng. - Cells Biomater., 2011, pp. 569–588, https://doi.org/10.5772/21983.
[49] P.O. Forest, R. Karoum, C.H. Gagnieu, Influence of gradual introduction of hydrophobic groups (stearic acid) in denatured atelocollagen on fibroblasts behavior in vitro, J. Biomed. Mater. Res. - Part A 80 (2007) 758–767, https://doi.org/10.1002/jbm.a.31042.
[50] K.S. Topp, B.S. Boyd, Structure and biomechanics of peripheral nerves: nerve responses to physical stresses and implications for physical therapist practice, Phys. Ther. 86 (2006) 92–109, https://doi.org/10.1093/ptj/86.1.92.
[51] G.H. Borschel, K.F. Kia, W.M. Kuzon, R.G. Dennis, Mechanical properties of acellular peripheral nerve, J. Surg. Res. 114 (2003) 133–139, https://doi.org/10.1016/S0022-4804(03)00255-5.
[52] J. Kim, D.H. Kim, K.T. Lim, H. Seonwoo, S.H. Park, Y.R. Kim, Y. Kim, Y.H. Choung, P.H. Choung, J.H. Chung, Charged nanomatrices as efficient platforms for modulating cell adhesion and shape, Tissue Eng. - Part C Methods. 18 (2012) 913–923, https://doi.org/10.1089/ten.tec.2011.0731.
[53] M. Dadsetan, A.M. Knight, L. Lu, A.J. Windebank, M.J. Yaszemski, Stimulation of neurite outgrowth using positively charged hydrogels, Biomaterials 30 (2009) 3874–3881, https://doi.org/10.1016/j.biomaterials.2009.04.018.
[54] A.J. Reid, M. Sun, M. Wiberg, S. Downes, G. Terenghi, P.J. Kingham, Nerve repair with adipose-derived stem cells protects dorsal root ganglia neurons from apoptosis, Neuroscience 199 (2011) 515–522, https://doi.org/10.1016/j.neuroscience.2011.09.064.
[55] C.R. Carvalho, J.M. Oliveira, R.L. Reis, Modern trends for peripheral nerve repair and regeneration: beyond the hollow nerve guidance conduit, Front. Bioeng. Biotechnol. 7 (2019), https://doi.org/10.3389/fbioe.2019.00337.